Aerodynamic Shape Optimization of Tailless Aircraft

Maurizio Milani

November 30, 2016

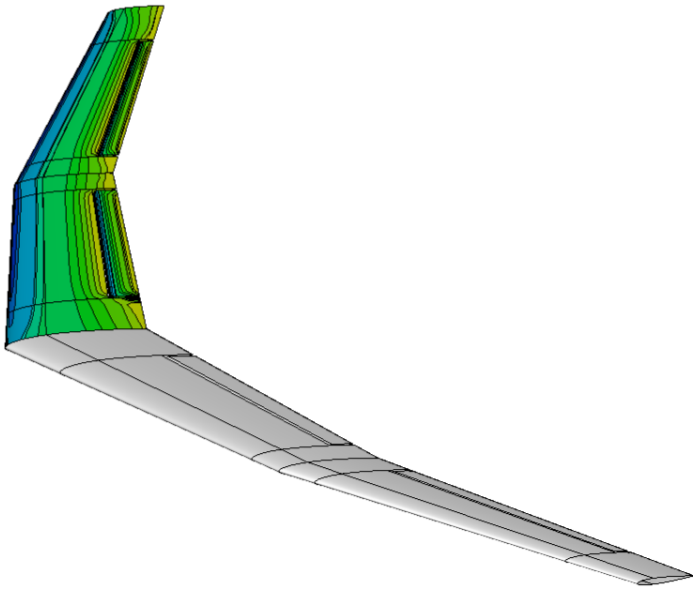

Faculty of Aerospace Engineering Politecnico di Milano

POLITECNICO DI MILANO

School of Industrial and Information Engineering

Master of Science in Space Engineering

Aerodynamic Shape Optimization of Tailless Aircraft

Supervisor : Prof. Lorenzo Trainelli

Second Supervisor : Dr. Giovanni Droandi

Author :

Maurizio Milani, Mat. 820513

Academic year 2015/2016

Ringraziamenti

Desidero ringraziare l'Ing. A. Abbà che con la sua passione e la sua intraprendenza ha ispirato l'argomento di questo lavoro di tesi.

Non da meno intendo ringraziare il Professor. L. Trainelli e l'Ing. G. Droandi, grazie alla loro disponibilità è stato possibile contare su un confronto sempre sincero e molto valido.

Abstract

This thesis presents a numerical method for designing an aircraft minimizing drag with a fixed level of static longitudinal stability. The method uses a genetic algorithm to reconfigure the aircraft through the minimization of a performance index consisting of trimmed drag evaluated at two flight conditions. Using this technique, tailless aircrafts are synthesized for minimum drag with acceptable stability margin. The method shows how low drag can be achieved by carefully choosing wing sweep, taper, and twist.

Keywords: Optimization, Tailless Aircraft, Mesh Generator, Genetic Algorithm, Drag Coefficient, Static Stability,Static Equilibrium

Nomenclature

Roman Symbols

$\overline{C}_D$	Drag coefficient	[-]
$\overline{C}_L$	Specified lift coefficient	[-]
$\overline{C}_l$	Local lift coefficient	[-]
$\underline{A}_0(u), \underline{A}_n(u), \underline{B}_n(u)$	Functions of surface coefficients	[-]
$\underline{C}_0^i, \underline{C}_n^i, \underline{S}_n^i$	Coefficients of Wing sections representation	[-]
$\underline{c}_0^m, \underline{c}_n^m, \underline{s}_n^m$	Coefficients of Wing sections representation	[-]
$\underline{dW}^i, \underline{ds}^m$	Difference functions	[-]
$\underline{R}(u,v)$	Remainder function	[-]
$\underline{s}^m(v)$	Derivative boundary conditions representation	[-]
$\underline{W}^i(v)$	Parametrically rapresentation of wing sections	[-]
$\widetilde{\underline{X}}(u,v)$	Approximate function of wing surface	[-]
ξ_{cg}	normalized center of gravity position	[-]
ξ_n	Normalized neutral point position	[-]
a	Smoothing parameter	[-]
b	Section span	[m]
$C_{L,\alpha}$	Lift coefficient derivative with respec to angle of attack	[-]
C_L	Lift coefficient	[-]
C_{M_P}	Profile pitching moment coefficient	[-]

C_{M_W}	Wash-out induced pitching moment coefficient	[-]
c_{mac}	Mean aerodynamic chord	[m]
$C_{Morigin,\alpha}$	Moment coefficient derivative with respec to angle of attack	[-]
c_{ref}	Refernce chord	[m]
c_{root}	Root chord	[m]
d_i	Actual value of the ith constraint	[-]
d_o	Constrained value of the ith constraint	[-]
K_p	Penalty weighting	[-]
M	N. of Fourier functions composing the series	[-]
m	Specified static stability margin	[-]
M_{CG}	Center of gravity moment	[-]
PF_i	Penalty functions	[-]
s_r, s_t	Boundary conditions parameters	[-]
u, v	Parameters which define a coordinate system on the surface	[-]
V_∞	Flow velocity	[m/s]
X_{cg}	Center of gravity position	[m]
X_n	Neutral point position	[m]
$\underline{X}$	Solution of Partial Differential Equation	[-]

Greek Symbols

δ_i	Flap deflection angle	[deg]
γ	Twist angle	[deg]
Λ	Quarter chord sweep	[deg]
λ	Taper ratio	[-]
ω	Smoothing parameter	[-]

ρ	Air density	$[kg/m^2]$
σ	Stability margin	[-]
S	Total wing surface	[deg]
Ω	Finite region of (u,v) parameters plane where the PDE are solved	[-]

Abbreviations

AR	Aspect Ratio
BREP	Boundary Representation
CS	Control Section
FBEI	First Best Individual
GA	Genetic Algorithm
GBO	Gradient Based Optimizator
LD	Lift Distribution
LTDR	Lift-to-Drag Ratio
MCS	Mesh Convengerce Study
MEG	Mesh Generator
OT	Optimization Tool
PDE	Partial Differential Equation
RG	Radar Graph

Contents

List of Figures

List of Tables

Chapter 1

Introduction

In the last years the interest for tailless and blended-wing-body aircrafts has grown a lot, seeing in these innovative configurations a way to improve the performance and mainly to reduce the fuel consumpion. Many books and articles speak about flying wing as the aircrafts of the future, most likely this will not happen, but for sure there are certain applications for which the flying wing principle is especially suited whilst for others it is not appropriate.[1]

A tailless aircraft (often tail-less) has no tail assembly and no other horizontal surface besides its main wing. The aerodynamic control and stabilization functions in both pitch and roll are incorporated into the main wing.

Theoretical advantages of the tailless configuration include low parasitic drag, low structures weight, manufacture simplification due to the lower number of part that compose these type of aircraft.

In the light of these characteristics it could be possible to say that tailless aircraft configuration is well suited to be used as a high efficient and light aircraft, such as any sailplane, glider or ultralight aircraft. The low aerodynamic drag is able to produce high lift-to-drag ratios, which is the main aspect when dealing with cross country races or simply long touristic sail flight.

Low weight, manufacture simplicity and easy on-ground handling, due to smaller size if compared to traditional aircraft, contribute to performance improvement and costs reduction.

Unfortunately there are also some consistent drawbacks in using such a configuration. Tailless plains suffer of trimming and control problems: difficult stable trimming, performances reduction due to stability requirements and difficulty in counteract adverse yaw.

It is probably for these and other reasons that in the history of flight there are

a few examples of successful tailless glider, such as: Horten flying wings [2], the SB-13 Arcus and the SWIFT ultra light foot-launchable sailplane. [3]

Horten brothers have been the pioneers of flying wings design, the Hortens designed some of the most advanced aircraft of the 1940s, including the world's first jet-powered flying wing, the Horten Ho 229. They made a lot of work and studies about performances improvement of tailless sailplane, in particular their work regarding this ambit of research culminated with the Ho IV, a high aspect ration sailplane used in competitions. This aircraft had a lot of advance features for that period but its performance, in term of LTDR for example, was not so excellent and was comparable with other traditional sailplanes of the period. This highlights the difficulties in designing a good flying wing using at the best its theoretically advantages on traditional aircraft.

More recent studies like the SB-13 Arcus confirm the complexity of the argument.

The above mentioned intrinsic drawbacks of tailless configuration have negative rebounds on design process and aggravate the development flow. In fact variables and parameters are numerous and their influence on aircraft's final features is highly non-linear and unintuitive.

In literature are present several articles speaking about aerodynamic shape optimization, mostly they are focused on wing optimization of traditional aircrafts, in general they analyze the problem considering already existent aircraft and using the optimization to increment the performance of the baseline wing and not to design an optimized one. Indeed they consider small changes with respect to baseline geometry taking in to account in this way the possibility to use gradient based optimizer. In particular in [4] the geometry of the baseline is changed only in the thickness, considering [5] the optimization is performed modifying the root and tip airfoil geometry, without considering ailerons deflection, fundamental in "real life" to trim the aircraft.

The study which is closer with the intentions of this thesis work is [6], in particular it goes further and includes in the optimization also a Stability Augmentation System. The weakness of this study is the fact that uses a 2D geometry to estimate the aerodynamic coefficients and it considers only simple trapezoidal wing.

Considering what was said above, the main goal of this thesis project is to develop an optimization tool able to manage automatically the flying wings design issues, optimizing the design variables in order to achieve the desired features and respect the constraints.

This tool will be used to design/optimize two configurations having different features and imposed constraints, in order to validate the new design procedure.

About aerodynamic simulation, a 3D panel method, COMPA, has been used. This code has been used to simulate the complete aircraft's aerodynamics in steady incompressible inviscid flow. It was developed at Politecnico di Milano by Dr. Giovanni Droandi. COMPA needs a pre-processor that generates the geometry, whose aerodynamic is simulated. The code used to represent the geometry has been developed in the ambit of this thesis project, it needs peculiar features such as versatility and robustness, that require pretty much effort to be achieved. For this reason its development has taken a big part of this thesis work.

The third main part, that constitutes the OT, is the optimizer. For practicality and easiness of use the entire work has been developed in Matlab, so the choice of the optimizer has been made between algorithms already implemented in Matlab platform: fmincon and Matlab Genetic Algorithm.

The choice has been made considering different factors, the most important of them has been the absence of information about solutions space, which could be constituted of several local minima, that became "dangerous" if not recognized.

When all the components were "ready" and available, the issue was to put them all together in the OT and to make it work well in such a way that it receives as inputs a 3D geometry to be optimized and some constraints to respect and comes out with the best compromise, which is complied with the designer requirements.

Outline of the Thesis Work

Chapter 2 : Pre-Processor Development. The chapter presents the theoretical principles which are used to develop the pre-processor. [7] It presents also the features of the pre-processor, in particular the dependency from boundary conditions. The procedure to include the flap in the wing mesh is analyzed and discussed regarding two different techniques. In the last part of the chapter the operation of the code is presented.

Chapter 3 : Aerodynamic Solver. A brief description of the aerodynamic solver is presented focusing the attention only on the features that are

important for this thesis work, the input and output principles and procedures and the reference system used.

Chapter 4 : Target Aerodynamic Characteristics. This chapter presents and discusses the aerodynamic characteristics involved in the optimization procedure, in particular a general description of drag composition, a brief analysis of static longitudinal stability and a more detailed discussion on flying wing trimming.

Chapter 5 : Optimization Procedure. The chapter describes in detail how the optimization cycle has been implemented and developed. In particular the choice of the optimization algorithm is discussed considering the pros and cons of the two alternative : gradient based algorithm or genetic algorithm. Variables are presented distinguishing between real optimization variables and parameters used to fix a certain baseline geometry. Constraints are discussed considering how they are implemented. In this chapter is also explained the procedure used to find the correct mesh thickness to obtain accurate results limiting the computational effort. At the end of the chapter is analyzed the operation of the optimization code, taking into account the program initialization, how the objective function is evaluated during an optimization cycle and how the optimization is stopped using a certain termination criteria.

Chapter 6 : Validation. This chapter discusses how the entire optimization tool is validated. The validation is made comparing the numerical results obtained from OT with theoretical results. In particular, a drag minimization on a rectangular wing is performed, considering as variables only the twist angles of some airfoil sections and constrained to have a certain C_L. The resulting span wise C_l distribution is compared with an elliptical one having the same wing C_L. Through an analyzsis of the results is possible to prove the efficacy of the code.

Chapter 7 : Application Studies. In this chapter two examples of "complete" optimizations are presented. All the variables presented in chapter 5 are considered and all the constraints are active. This chapter analyzes the optimization procedure from the point of view of the objective function component trends, during the iterations and looking at the final geometry compared with the initial one.

Chapter 8 : Conclusions and Future Developments. All the results and limitations are summarized in this chapter, some future developments are

prescribed in order to complete and improve the OT developed in this thesis work.

Chapter 2

Pre-Processor Development

The "mesh generator" used in the optimizing cycle has been entirely developed in the thesis project. This choice was driven by the peculiar features needed to make it compatible with an automatic optimizing process, and to ensure the possibility to represent a lot of types of wing shape, in order to do not limit the admissible solutions space.

The code must be able to reduce a complex geometry, like the one of a wing, in a number of parameters (possibly a small number), which are able to uniquely determine a certain geometry.

In order to achieve good estimation of aerodynamic coefficients, the mesh maker must be able to distribute the mesh in particular ways. These mesh patterns guarantee good results with the lowest possible computational effort, reducing also the simulation time.

A method is presented for generating a parametric surface given two-dimensional section data. It is an extension of a method for the efficient parametrization of complex three-dimensional shapes called the PDE method. The method views surface generation as a boundary-value problem and produces surfaces as solutions of elliptic partial differential equations.

2.1 Outline of the PDE Method

Unlike conventional systems, the method is based upon a view of surface generation as a boundary value problem in which each surface patch is defined by data defined along the character lines which form the patch boundaries. Adjacent surface patches share common boundary conditions and thus continue to meet exactly throughout any changes to the overall geometry that may oc-

cur during the design process.This is in contrast to conventional conventional Boundary Representation (BREP) systems which typically use surface patches generated from polynomial spline functions, and tend to require 'trimming' at the boundaries where adjacent patches meet. Also, far fewer surface patches are usually required using the PDE method than a spline-based approach.

Past work has concentrated upon solutions to the following equation,

$$\left(\frac{\partial^2}{\partial u^2} + a^2 \frac{\partial^2}{\partial v^2} \right)^2 \underline{X} = 0 \tag{2.1}$$

This equation is solved over some finite region Ω of the (u, v) parameter's plane, subject to boundary conditions on the solution which usually specify how $\underline{X}$ and its normal derivative $\partial \underline{X}/\partial n$ vary along $\partial\Omega$.

The three components of the function $\underline{X}(x(u,v), y(u,v), z(u,v))$are the Euclidean coordinate functions of points on the surface, given parametrically in terms of the two parameters (u, v) which define a coordinate system on the surface. Note that in the simplest cases (3.1) is solved independently for the x, y and z coordinates.

The boundary conditions on $\underline{X}$ which we shall refer to as function boundary conditions, determine the shape of the curves bounding the surface patch in physical space, or, more specifically, their parametrization in terms of (u, v). The boundary conditions on $\partial \underline{X}/\partial n$, which we shall refer to as derivative boundary conditions, basically determine the direction in physical space in which the surface moves away from a boundary and how 'fast' it does so.

The partial differential operator in (3.1) represents a smoothing process in which the value of the function at any point on the surface is, in a sense, an average of the surrounding values. In this way a surface is obtained as a smooth transition between the boundary conditions imposed on the function and its first derivative. The parameter a controls the relative rates of smoothing between the (u, v) parameter directions.

2.2 Interpolating Wing Sections

Consider the problem of generating a smooth wing-surface that passes through 2N two-dimensional wing sections which are specified. Suppose for the moment that each wing section $\underline{W}^i(v)$ is given parametrically as a vector-valued function of a periodic coordinate v that runs around the wing,

$$\underline{W}^i(v) = \left(W_x^i(v), W_y^i(v), W_z^i(v)\right) \tag{2.2}$$

where the sections $i = 1, 2N$ correspond to the ends of the wing, and W_z^i is the specified span-station of the ith section. In what follows below we will assume that the x coordinate is approximately aligned with the wing chord and the y coordinate is aligned with the wing thickness. In previous work: the order of the partial differential equation was kept as low as possible consistent with the requirements of surface control and continuity at patch boundaries. Here, for reasons that will become clear below, we will consider solutions of the equation

$$\left(\frac{\partial^2}{\partial u^2} + a^2\frac{\partial^2}{\partial v^2}\right)^{(N+1)} \underline{X} = 0 \tag{2.3}$$

Now consider the solution $\underline{X}(u,v)$ of Eq. (3.3) over the (u,v) region Ω : $[0,1] \times [0,2\pi]$, subject to periodic boundary conditions in the u direction. Topologically, the surface is like a closed 'band' with the $u = 0$ and $u = 1$ isoparametric lines corresponding to the wing-sections $\underline{W}^1(v)$ and $\underline{W}^{2N}(v)$, respectively, which will form the boundary curves for the surface patch. If we assume for the moment that the boundary conditions for Eq. 2.3 take the form

$$\begin{aligned} \underline{X}(0,v) &= \underline{W}^1(v), \\ \underline{X}(1,v) &= \underline{W}^{2N}(v), \end{aligned} \tag{2.4}$$

$$\begin{aligned} \underline{X}_u(0,v) &= s^0(v), \\ \underline{X}_u(1,v) &= s^1(v), \end{aligned} \tag{2.5}$$

where $\underline{W}^1(v)$ and $\underline{W}^{2N}(v)$ are of the form Eq. 2.2, and the derivative functions $s^0(v)$ and $s^1(v)$ are specified, then, by using the method of separation of variables, the solution to Eq. 2.3 may be written in closed-form thus

$$\underline{X}(u,v) = \underline{A}_0(u) + \sum_{n=1}^{M} \{\underline{A}_n(u)\cos(nv) + \underline{B}_n(u)sin(nv)\} \tag{2.6}$$

where, depending on the boundary conditions, M may be infinite. The 'coefficient' functions $\underline{A}_n(u)$ and $\underline{B}_n(u)$ are of the form

$$\underline{A}_0(u) = \underline{a}_{00} + \underline{a}_{01}u + \underline{a}_{02}u^2 + \cdots + \underline{a}_{0(2N+1)}u^{2N+1} \tag{2.7}$$

$$\begin{aligned}\underline{A}_n(u) &= \underline{a}_{n(2N+2)}u^{2N+1}e^{anu} + \underline{a}_{n(2N+1)}u^{2N+1}e^{-anu} + \underline{a}_{n(2N)}u^{2N}e^{anu} \\ &\quad + \underline{a}_{n(2N-1)}u^{2N}e^{-anu} + \cdots + \underline{a}_{n2}e^{anu} + \underline{a}_{n1}e^{-anu}\end{aligned} \tag{2.8}$$

$$\begin{aligned}\underline{B}_n(u) &= \underline{b}_{n(2N+2)}u^{2N+1}e^{anu} + \underline{b}_{n(2N+1)}u^{2N+1}e^{-anu} + \underline{b}_{n(2N)}u^{2N}e^{anu} \\ &\quad + \underline{b}_{n(2N-1)}u^{2N}e^{-anu} + \cdots + \underline{b}_{n2}e^{anu} + \underline{b}_{n1}e^{-anu}\end{aligned} \tag{2.9}$$

and $\underline{a}_{n(2N+2)}, \underline{b}_{n(2N+2)}$ etc. are constant vectors. Now, since the wing-sections are periodic in the variable u, we can express them as Fourier series thus

$$\underline{W}^i(v) = \underline{C}^i_0 + \sum_{n=1}^{M} \left\{ \underline{C}^i_n \cos(nv) + \underline{S}^i_n sin(nv) \right\} \quad i = 1, \ldots, 2N \tag{2.10}$$

where the $\underline{C}^i_n, \underline{S}^i_n$ are the Fourier coefficients. We will ignore for the moment the fact that the Fourier sum in 2.10 may be infinite, and consider first the case where each wing-section is expressible as a finite Fourier series. Now suppose that the derivative boundary conditions can be expressed in a similar form to Eq. 2.10, i.e.

$$\underline{s}^m(v) = \underline{c}^m_0 + \sum_{n=1}^{M} \{ \underline{c}^m_n \cos(nv) + \underline{s}^m_n sin(nv) \} \quad m = 0, \ldots, 1 \tag{2.11}$$

We wish to find a PDE surface of the form given by Eq. 2.6, that interpolates the given wing-sections and which also satisfies the derivative boundary conditions 2.4 and 2.5. Now, the number of Fourier terms in the derivative boundary conditions Eq. 2.11 and wing sections Eq. 2.10, and the number of coefficients in the separable solution given in Eqs. 2.8 and 2.9, is such that associated with each frequency term in Eq. 2.6 ($cos(nv)$ say) there are $2N + 2$ Fourier coefficients in Eq. 2.8 to find, and $2N + 2$ conditions on those coefficients obtained from the Fourier expansions 2.10 and 2.11 of the specified wing-sections and boundary conditions. Thus one may form a system of algebraic equations for each Fourier frequency which is of the form

$$\mathbf{A}\underline{g} = \underline{h} \tag{2.12}$$

where g is a vector whose components are the coefficients $\underline{a}_{ij}$ or $\underline{b}_{ij}$ of Eqs. 2.7, 2.8, or 2.9, $\underline{h}$ is a vector whose components are derived from the corresponding Fourier coefficient of the specified $2N$ wing-sections and 2 derivative boundary-conditions, and $\mathbf{A}$ is a $(2N+2)x(2N+2)$ matrix whose entries are obtained from the condition that the surface interpolate the wing-sections at specified values of u and satisfies the boundary conditions. In forming this system of equations one must decide how the interpolating wing surface should be parametrized in the u direction, i.e. decide at what value of u each span-station W_z^i: lies. Obviously, the end sections lie at $u = 0,1$, while the intervening sections lie at intermediate values, of u.

Although rather involved, Eq. 2.12 may be solved using an algebraic manipulator, or else it may be solved numerically. The solution of this set of equations may be used in conjunction with Eq. 2.6 to yield an analytic expression for a surface that interpolates the given wing-sections, assuming that they can be represented by finite Fourier series. All well and good. But, for an arbitrary selection of wing sections, even assuming that they can be expressed in terms of functions in closed-form, it is by no means inevitable that they can be expressed as finite Fourier series. However, the procedure outlined above can be modified in the following way to cover this more general situation.

Assume that the wing-sections and the derivative boundary conditions can be written thus,

$$\underline{W}^i(v) = \underline{C}_0^i + \sum_{n=1}^{M} \left\{ \underline{C}_n^i \cos(nv) + \underline{S}_n^i sin(nv) \right\} + \underline{R}_w^i(v) \quad i = 1,\ldots,2N \tag{2.13}$$

$$\underline{s}^m(v) = \underline{c}_0^m + \sum_{n=1}^{M} \{ \underline{c}_n^m \cos(nv) + \underline{s}_n^m sin(nv) \} + \underline{R}_s^m(v) \quad m = 0,\ldots,1 \tag{2.14}$$

i.e. as the sum of a. finite Fourier Series to M terms plus 'remainder' functions $\underline{R}_w^i(v)$ or $\underline{R}_s^m(v)$ which contain the higher-order Fourier modes.

The basic idea is to choose a value for M in Eqs. 2.13 and 2.14, approximate the wing-sections and boundary conditions by a finite Fourier series representation, ignoring the remainder functions, and use the procedure described above to

generate a wing-surface $\underline{\widetilde{X}}(u,v)$ that interpolates these 'approximate' sections and satisfies the 'approximate' boundary conditions. Then define the following $(2N+2)$ 'difference' functions

$$\underline{dW}^i(v) = \underline{W}^i(v) - \underline{\widetilde{X}}(u_i,v) \quad for\, i = 1,\ldots,2N \tag{2.15}$$

$$\underline{ds}^m(v) = \underline{s}^m(v) - \underline{\widetilde{X}_u}(m,v) \quad for\, m = 0,\ldots,1 \tag{2.16}$$

Next, to obtain a wing-surface $\underline{X}(u,v)$ that interpolates is defined the actual wing-sections, the following function

$$\begin{aligned} \underline{R}(u,v) \;=\; & \underline{r}_{(2N+2)}(v)u^{2N+1}exp(\omega u) + \underline{r}_{(2N+1)}(v)u^{2N+1}exp(-\omega u) + \\ & + \underline{r}_{n(2N)}(v)u^{2N}exp(\omega u) + \underline{r}_{(2N-1)}(v)u^{2N}exp(-\omega u) \\ & + \cdots + \underline{r}_2(v)exp(\omega u) + \underline{r}_{n1}(v)exp(\omega u) \end{aligned} \tag{2.17}$$

which is required to satisfy the conditions

$$\underline{dW}^i(v) = \underline{R}(u_i,v) \quad for\, i = 1,\ldots,2N \tag{2.18}$$

$$\underline{ds}^m(v) = \underline{R}_u(m,v) \quad for\, m = 0,\ldots,1 \tag{2.19}$$

of which there are sufficient to determine the $(2N+2)$ functions $\underline{r}_1(v),\ldots,\underline{r}_{(2N+2)}(v)$ in Eq. 2.17.

Finally $\underline{X}(u,v)$ is given by

$$\underline{X}(u,v) = \underline{\widetilde{X}}(u,v) + \underline{R}(u,v) \tag{2.20}$$

This procedure can be viewed as a means of generating an approximate solution 2.20 to Eq. 2.3 that exactly satisfies the boundary conditions and interpolates the specified wing-sections (to within machine accuracy).

The choice of M will obviously affect how good an approximation 2.20 is to the actual solution of Eq. 2.3. Depending on the variation in the shape of the wing-sections to be interpolated, the choice of a can have an important influence on the smoothness of the interpolating surface.

2.3 Meshing Features and Procedures

2.3.1 Smoothing Parameters and Boundary Conditions

The implementation of the MEG has been done rigorously following the procedure and the formulas explained before.The method is robust and versatile but is very important to correctly tune the parameters, in order to obtain smooth shapes without spur fluctuations. It is also important to correctly manage the boundary conditions which are able to consistently modify the regions near by the tip and root of the wing.

The derivative boundary conditions are taken to be :

$$\begin{aligned} \underline{s}^0(v) &= \underline{c}_0^0 + \sum_{n=1}^{M} \left\{ \underline{c}_n^0 \cos(nv) + \underline{s}_n^0 sin(nv) \right\} \\ \underline{s}^1(v) &= \underline{c}_0^1 + \sum_{n=1}^{M} \left\{ \underline{c}_n^1 \cos(nv) + \underline{s}_n^1 sin(nv) \right\} \end{aligned} \tag{2.21}$$

in which :

$$\underline{c}_0^0 = -s_r \cdot \underline{C}_0^0 \qquad \underline{c}_n^0 = -s_r \cdot \underline{C}_n^0 \qquad \underline{s}_n^0 = -s_r \cdot \underline{S}_n^0$$

$$\underline{c}_0^1 = -s_t \cdot \underline{C}_0^{2N} \qquad \underline{c}_n^1 = -s_t \cdot \underline{C}_n^{2N} \qquad \underline{s}_n^1 = -s_t \cdot \underline{S}_n^{2N}$$

where the magnitudes of parameters s_r and s_t control the "speed of the surface" when it departs from boundary curves and their sign determines the direction of departure.

In fact the wing shape is created interpolating a certain number of airfoils distributed along the half wingspan, in particular the right half wing. In this way the result is an half wing in which the boundaries are the root and the tip airfoil.

Once the space coordinates of the points that constitute the right half wing is generated, using a simple mirroring operation the full wing shape is created.

Below some Figures will be shown, they illustrate the boundary conditions influence.

All the images are generated considering surfaces with the same geometrical parameters but with different boundary conditions.

From the Figures 2.1, 2.2, 2.3 is possible to notice how the parameter s_t is more effective in surface modification.

As said in Section 2.2 , the BC are used to ensure the smoothness between different surface patches. In this thesis work only single patch surfaces has

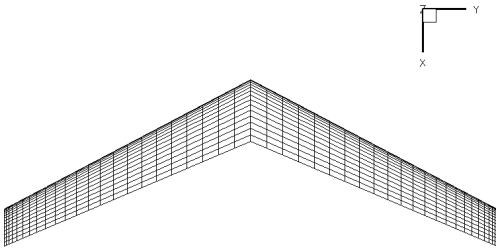

Figure 2.1: Boundary conditions influence having $s_r = 0, s_t = 0$.

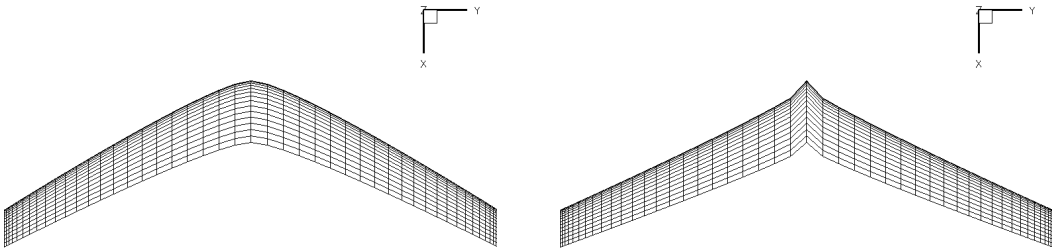

Figure 2.2: Boundary conditions influence having $s_r = 10, s_t = 0$ for the figure on the left and$s_r = -10, s_t = 0$ for the figure on the right.

been used, so there is no need to impose particular BD. They were put all to zero, which means that the surface departs from boundary airfoils (root and tip) in perpendicular directions and with zero velocity.

Here is used the same wing surface used above for boundaries conditions comparisons.

The Figure 2.4 shows how with a lower smoothing parameter a the surface is plenty of spur fluctuations.

The smoothing parameters (a, ω) were chosen using a trial and error procedure in order to mitigate spur fluctuations. In general the parameters (a, ω) are specific for each type of geometry, in theory there is a set of parameters for every new surface, in practice they remain constant for a family of similar wing shape without degrade the results.

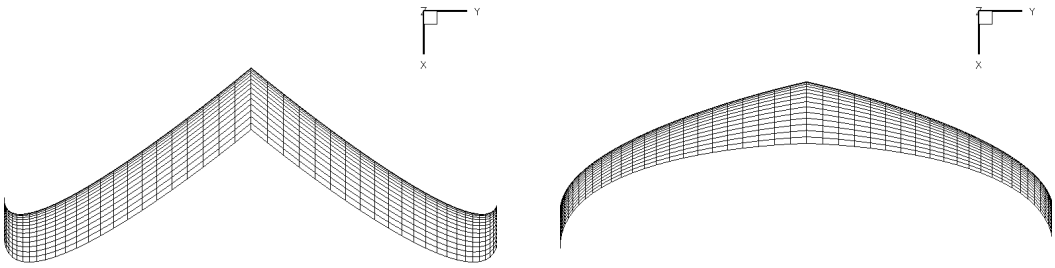

Figure 2.3: Boundary conditions influence having $s_r = 0, s_t = 2$ for the figure on the left and$s_r = 0, s_t = -2$ for the figure on the right.

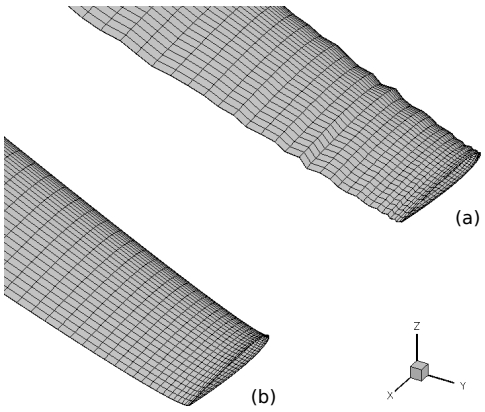

Figure 2.4: Smoothing parameters $a = 0.01, w = 0.5$ for surface (a) $a = 0.1, w = 0.5$ for surface (b).

Refer to Table 2.1 for the numeric values of BC and smoothing parameters.

s_r	s_t	a	w
0	0	0.1	0.5

Table 2.1: Settings parameters.

2.3.2 Mesh Distribution

In order to achieve the best simulation results with the minimum number of grid points it has been necessary to correctly manage the mesh, thickening it where the surface curvature is high. The mesh has to be thickening also at the wing tip, in fact this region is where the vorticity generate the induced drag,

which is important to properly assess. Refer to Figure 2.5.

The sections used to interpolate the wing shape are generated using a code that knowing the four digits of a NACA airfoil give as output a collection of points coordinates (x, y). This points can be distributed along the profile in many different ways. In particular using an half-cosine distribution centered in the leading edge, it is possible to considerably reduce the number of points to well represent the profile.

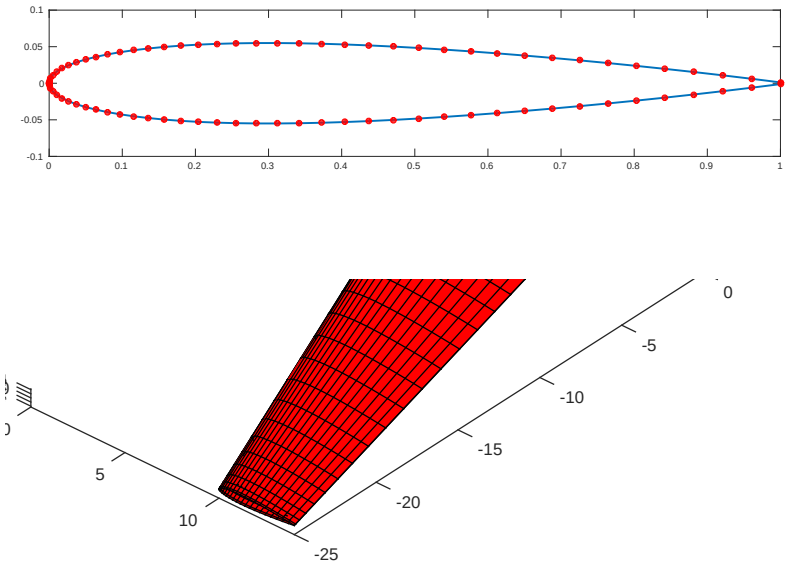

Figure 2.5: NACA 0011 airfoil generated using a cosine distributions of points and cosine distribution of panels in wingspan direction.

The distribution of the panels [1] in the chord direction is given by the distribution of the points that constitute the sections to be interpolated. The mapping between x, z coordinates (real space) and v coordinate is determined simply by the relation that exist between reference sections coordinates and v values. For example if the values of v are considered all equidistant and x, z coordinates of the airfoil points are half-cosine distributed considering the curvilinear abscissa, a constant increment in v correspond to half-cosine increment in real space.

In wingspan direction it is a bit more complex. In fact the mapping between y coordinate (real space) and u coordinate is determined by the solution of PDE. One can think at u like a time coordinate and y like a space coordinate

[1] the panel is the plain surface that has like vertices four mesh points

which follows a law of motion that is the solution of the PDE used to generate the surface. The problem has been solved using an iterative process, given the desired y distribution, it returns the correct u values.

Some other issues needed to be addressed during the development of the code: it was necessary to create a routine that check the distance between consecutive wing sections, if there are two sections whose distance to each other is under a certain tolerance, the routine deletes one of them. It is necessary because during aerodynamic simulation, if two points are too close, the solution diverge and assumes not feasible values. The panels distribution in y direction is influenced by the presence of the ailerons, it has to be thickening near the gaps between wing and ailerons, in order to have good simulation results.

2.3.3 Flap Insertion

For sure the main issue related with the MEG has been the necessity to insert in the wing some movable surfaces. They have to be separated from the rest of the wing in order to simulate the losses generated by the gaps between the wing and the flaps, they have to be rotated without intersect the fixed surface and without get too close to it. The panels distribution in chord and wingspan direction has to be adapted to consider the presence of the flaps.

Initially a big work has been made trying to embed the flaps in the wing without any gap between the two surfaces. It was made to simplify the flaps insertion without affect too much the simulation realism. Refer to Figure 2.6.

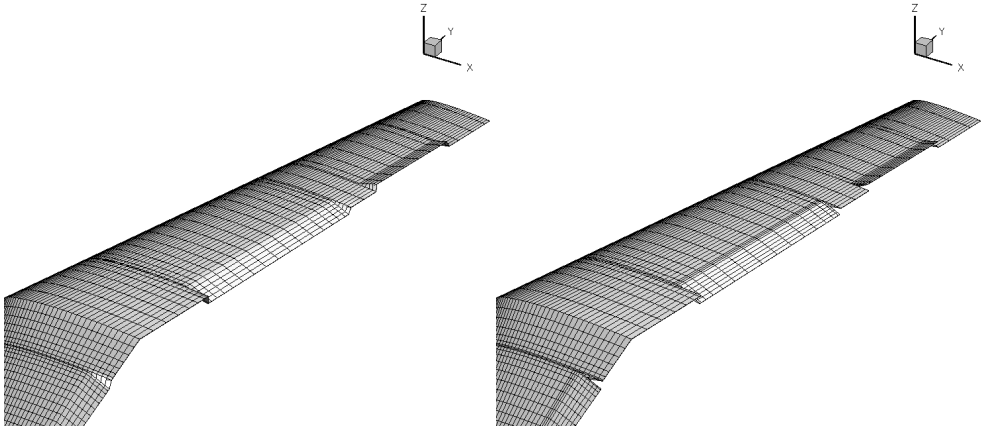

Figure 2.6: Example of flaps insertion without gap, figure on the left shows a flap completely attached to the wing, instead figure on the right shows a flap with lateral gaps. These are two solutions that have been tried.

Difficulties were encountered because trailing edge modifications where the

flaps have to be placed, lead to non desired changes in other parts of the surface. This happens due to the intrinsic features of PDE method, which is a sort of interpolation, for this reason a small change in a confined part can produce modifications in all the domain.

Looking at image (c) of Figure 2.7 , the regions where the surface is irregular, show the differences between the two wings. It is possible to notice that big differences are present near by the trailing edge due to the ailerons deflection, but also near by the leading edge the surfaces are changed. This is caused by interpolation issues mentioned above.

In order to avoid aforementioned interpolation problems, the wing is in principle generated without any aileron, then a trimming procedure separates the parts adding the leading edge at the flap. It has a cylindrical shape trimmed in order to generate a smooth connection between upper and lower flap surface. At this point the panels distribution along the chord of the flap is re-interpolated in order to achieve the best fit for the new configuration. Now is possible to rotate the flap, the rotation axis considered for each movable part is the line that connect the centers of flap boundary sections leading edges. Refer to Figure 2.8.

A very important aspect of the code that generates the aileron, is the capability of re-distribute the panels dimensions independently. This is made in order to reduce spurius oscillations of the aerodynamic solution near by the regions where the flap is closest to the fixed wing.

In Figure 2.9 is easy to notice how the code has been able to redistribute the mesh panels in order to adjust the mesh at different aileron configurations.

2.3.4 Code Operation

As seen in Chapter 2, briefly speaking the code works interpolating a certain number of airfoils in order to obtain a loop surface having like control sections the airfoils interpolated. In fact the surface passes perfectly through the control sections trying to obtain a smooth shape between two consecutive CS.

The code operation is simple and it starts passing to it the coordinate of the CS. The sections can be oriented in the space as you want, translated and rotated along all the three coordinate axes, the sequence used by the code to interpolate the sections must be provided by the operator. The sequence is given entering the x, y, z coordinates of each airfoil in three different matrices,

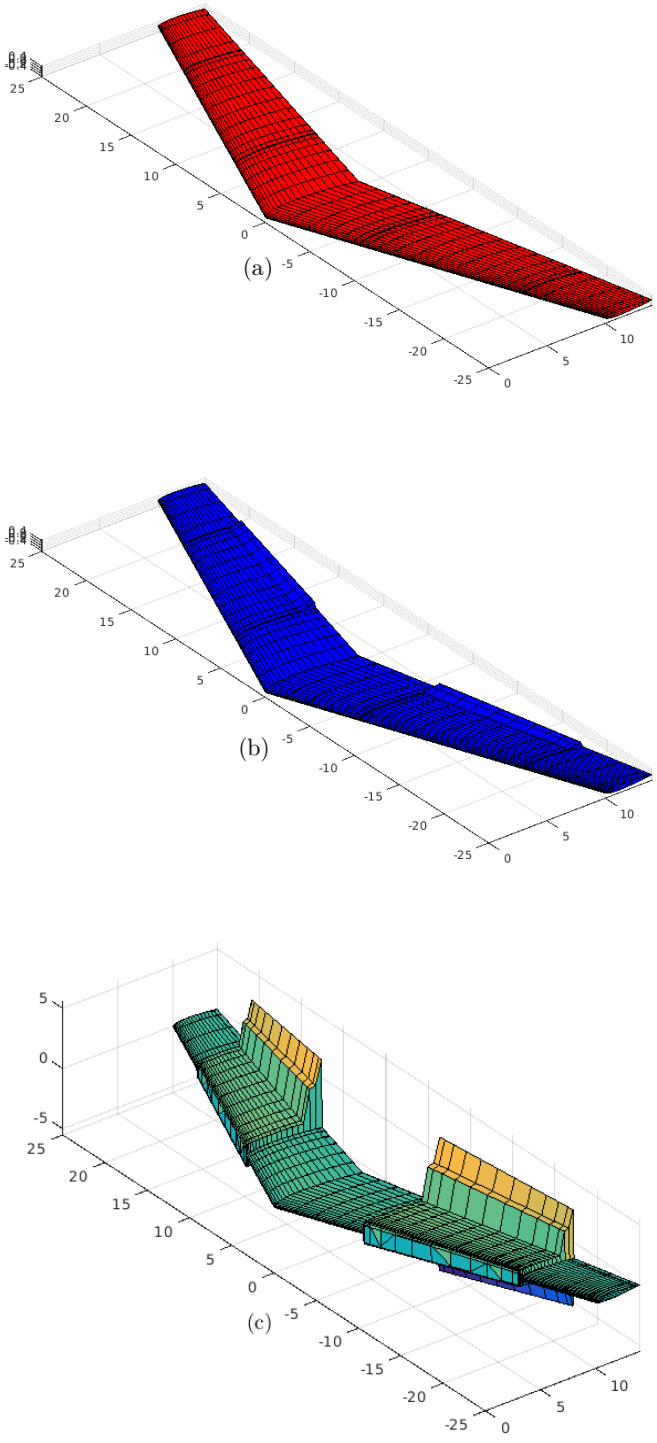

Figure 2.7: (a) Wing with zero flap angle $\delta = 0°$ (b) Wing with flap deflected $\delta = 20°$(c) Comparison between the wing with $\delta = 0°$ and $\delta = 20°$.

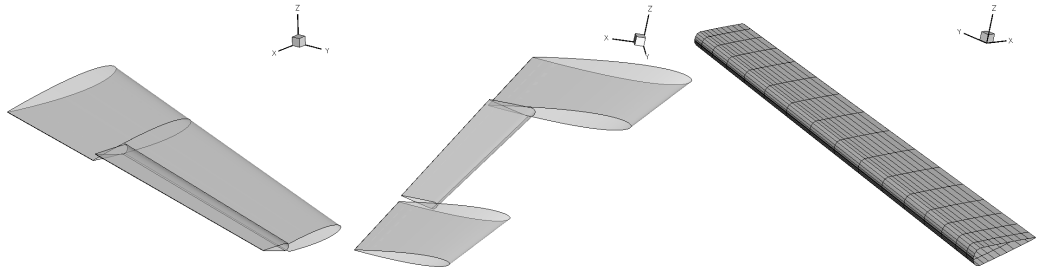

Figure 2.8: Examples of wing with a single flap, the image on the right shows the flap alone.

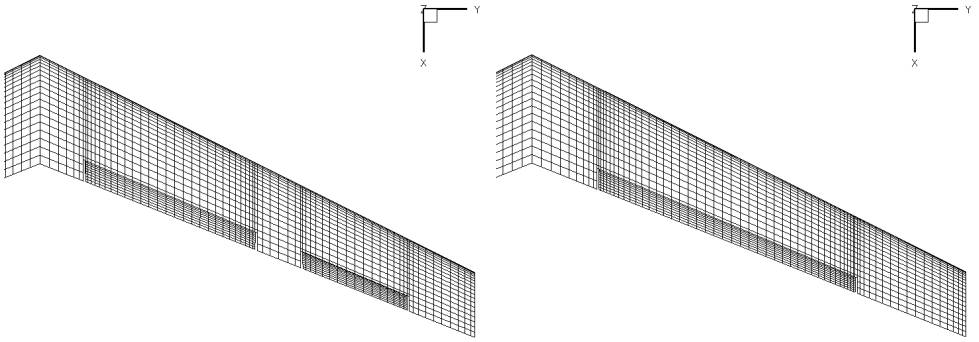

Figure 2.9: Examples of different aileron configurations.

each airfoil coordinates constitute a row of the matrix. In this way the code starts the interpolation from the first row and continuing down till the last.

The procedure described above is used when you need to generate a wing with any kind of geometry, for what regards this thesis work the wings used in the simulations are trapezoidal wings. They are composed only by one patch or assembled by a certain number of trapezoidal surfaces. This means that the control sections needed for one trapezoidal surface are only two.

Anyway the code is made for reading as input a matrix with all the sections together, it does not matter if the wing is composed by one or more patches.

For what concern the ailerons, they are inserted using the dimension and the position of each one supplied to the code by vectors. There is a vector that contain the y coordinates of starting points of each flap (s), another one that contain the length of the flap (l) in y direction and the last one that contain the deflection angles δ. Refer to Figure 2.10.

The chord dimension of the flaps is supplied in another vector considering a certain percentage of the total wing chord. So if the chord of the wing vary

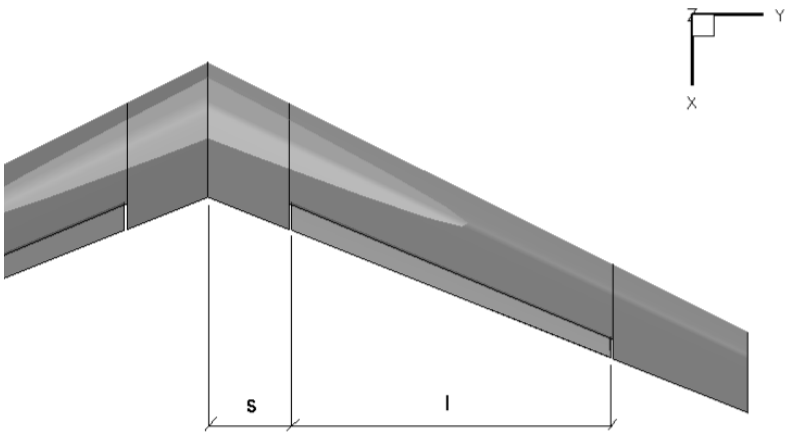

Figure 2.10: Scheme of flap dimensions.

along the wingspan, the chord of the flaps vary proportionally to it.

Other two important dimensions can be set, They are the gap between ailerons leading edge and the wing fixed part ($gap2$) and the gaps between the flap and the fixed wing in wingspan direction ($gap1$). Refer to Figure 2.11.

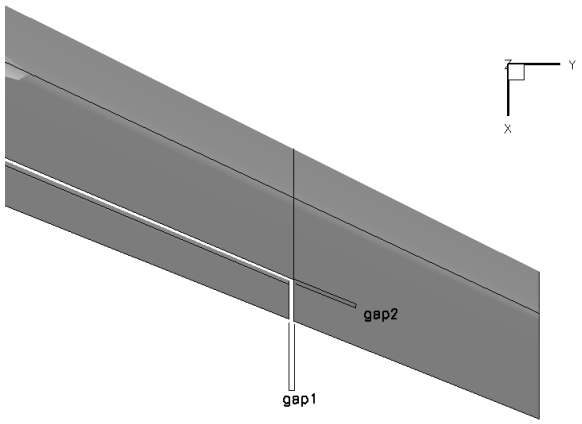

Figure 2.11: Scheme of mutual position between flap and fixed wing part.

The user must also choose the number of mesh panels in chord direction for fixed wing and ailerons separately, and the number of mesh panels in wingspan direction no matter of the number and dimension of the ailerons. The code distributes the panels in the best way to fit with the wing configuration.

Chapter 3

Aerodynamic Solver

3.1 Introduction

COMPA is a boundary elements (panels) numeric code used to simulate the aerodynamic of wings and other bodies in steady incompressible flow ([8], [9], [10]). The code admit the possibility to consider a certain number of BODIES each one composed by BLOCKS.

The global aerodynamic coefficients are computed summing the effects of the BLOCKS that compose a BODY.

3.2 Numerical Scheme

3.2.1 Virtual Singularity for Lift BODIES

About lift BODIES (wings) are used vortices and sources together, vorticies are distributed on external surface instead sources are placed on "middle surface" (is the surface placed between upper and lower part of the wing). The vortices are placed on the panels to generate a ring along all the perimeter (a Vortex Lattice that enclose all the body's external surface). The influence formulas used are that proposed by Muck but with appropriate vectors operations instead of using trigonometric functions.

The trailing edge panels pair vorticies are not closed in a ring but the trailing edge part of the panel perimeter is without vorticies (like a stirrup) in order to impose the Kutta condition. The semi-infinit longitudinal vorticies that complete the stirrup are placed along asymptotic velocity direction.

3.3 Code Organization

The code read a "mesh file" that contain the geometry of the bodies (filename.msh) and starts to compute the necessary geometric parameters (areas, panels perpendicular directions, placing points) for each panel. The influence coefficients are calculated end organized in a matrix formed by three square sub-matrices, each one of that contain the influence coefficients along one of the coordinates directions.

The code need the angle of attack and the yaw angle in order to add at the solution the effect of the wake. The system matrix is obtained multiplying the influence matrices and the panels perpendicular vectors summing, at this point, the effect of the wake.

When the system is solved, each sub-matrix gives the velocities in the coordinate directions. Composing the three velocities is possible to recover the velocity of the flow over the body and at the same time also the pressures and the forces.

The linear system is solved using the conjugated gradients technique.

3.4 Input and Output

The code reads the geometry from the mesh file, produce the influence matrices and then read from *filename*.inp the attitude and the options that have to be used in the computation. The outputs are different files, the most relevant for this thesis work are the *filename*.txt that contains the force and moment coefficients and the file that contains the distribution of pressure and velocity on each body that compose the tested geometry.

As said before using the file *filename*.inp is possible to impose some options, one of them is the "symmetry" that allows the user, if the simulated geometry have a plane of symmetry, to pass at the code only half geometry. Reducing considerably the computational effort.

From COMPA output file (*filename*.txt) the aerodynamic coefficients are extracts using the MATLAB "*importdata* function".

3.5 Reference System

COMPA, in order to interpret the mesh points and to calculate the aerodynamic coefficients, uses a its own reference system. The moment coefficients

are calculated in the origin of the system.

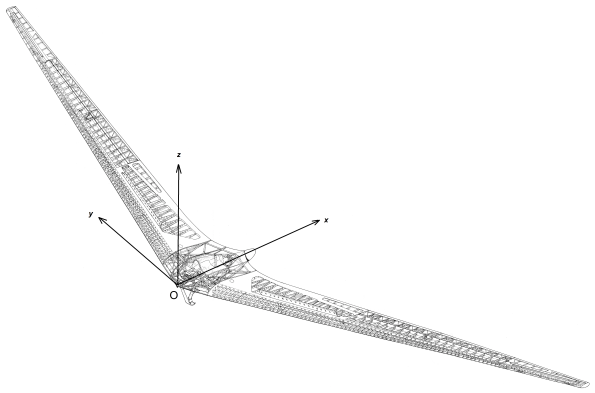

Figure 3.1: Reference system used by COMPA.

COMPA used a reference system centered in the leading edge of the wing, with the x axis that points to trailing edge, y axis that points in wingspan direction with the positive part that lays on right wing and the z axis, obtained using the right hand rule, with the positive direction that points towards the upper part of the wing, refer Figure 3.2.

Chapter 4

Target Aerodynamic Characteristics

4.1 Drag

In this section an overview of the aerodynamic drag will be presented . The performance estimation, which is of major importance for the optimization, will largely depend on the correct calculation of the drag. As an introduction, some attention will be spend on how all drag components are defined in further discussions. As there are a lot of different ways in which drag is subdivided, it is important to create an insight on how they are used in this document.

4.1.1 Overview

In an aircraft drag polar it is customary to distinguish two different types of drag, a lift independent part also referred to as zero lift drag and a lift dependent part. However it is mostly unclear what they are composed of and how they are influenced. Lets start with a breakdown of the overall drag:

$$\begin{aligned} D &= C_D qS = C_{Dp} qS + C_{Di} qS, \\ &\Downarrow \\ C_D &= \frac{D}{qS} = C_{Dp} + C_{Di} \\ & \quad pC_L^2 + k\frac{C_L^2}{\pi A} \\ & \quad C_{D0} + k\frac{C_L^2}{\pi A} \end{aligned} \tag{4.1}$$

The profile drag is the total drag of the wing minus the induced drag. This drag can be subdivided into airfoil friction drag and pressure drag. Friction drag is the component of the forces tangential to the airfoil surface, acting in the direction of the flow. This component only exist if the aerodynamic calculations on the airfoil incorporate viscous effects. The pressure drag is the component of the forces normal to the surface, in the direction of the flow. A part of this drag is constant and will be added to C_{D0} , while the other part varies with the lift and is incorporated in the second term of Eq. 4.22.

This second term is often referred to as "induced drag", it would be better to refer to it as the lift dependent drag. The Oswald factor, e, combines the induced drag factor, k, and the profile drag factor, p:

$$e = \frac{1}{k + p\pi A} \tag{4.2}$$

For what concern the OT implemented in this thesis work, the drag considered is the sum of induced plus pressure profile drag. It means that during the optimization the objective function take care about of the drag due to lift distribution over the span wise direction C_{Di} and also the drag due to the shape of the wing and its angle of attack C_{D0} (Ex. cross section area)

4.2 Static Longitudinal Stability

The way of treating stability for a flying wing is no different from large aircraft. The focus of this section will be on the pitch stability, as this is critical for tailless aircraft configuration. Sweep, which is required for trimming the aircraft as will be explained later in this section, will also increase the directional stability. Dynamic stability is hard to determine as the values for the stability derivatives are badly estimated using 3D panel method. A better way to approach this problem is to optimize the design and determine these values in a wind tunnel or with advanced CFD methods and then make small changes to the design to ensure dynamic stability

The static longitudinal stability is determined by the stability margin. This stability margin is defined by the difference between the aircraft neutral point and the location of the center of gravity. For a tailless aircraft this simplifies to the location of the wing aerodynamic center with respect to the aircraft center of gravity. Eq. 4.24 provides a mathematical description of this stability margin.

$$\sigma = \frac{(X_n - X_{cg})}{c_{ref}} = \xi_n - \xi_{cg} \tag{4.3}$$

X_{cg} is the center of gravity position along x axis. X_n is the position of wing neutral point and c_{ref} is the mean aerodynamic chord. ξ_n, ξ_{cg} are the chord normalized center of gravity and neutral point positions.

In this equation the location of the center of gravity, X_{cg} , is determined by the location of the components inside the aircraft. When the stability margin is positive ($\sigma > 0$), the aircraft will be stable. The aircraft is neutrally stable when the location of the center of gravity is the same as the neutral point, which explains its name. A negative value results in an unstable aircraft. The reference chord length is taken equal to the wing mean aerodynamic chord, and can be calculated with,

$$c_{mac} = \frac{2}{S_{ref}} \int_0^{b/2} c^2(y) dy \tag{4.4}$$

, in which $c(y)$ represents the chord length at spanwise location y.

The only remaining value to be determined in Eq. 4.24 is the location of the neutral point. The neutral point stick fixed, is in essence the same as the aerodynamic center of a complete aircraft. The definition of this neutral point is the following:

The longitudinal location, when taken as the reference point[1] *through which the aerodynamic forces act, in which the pitching moment of the complete aircraft is independent of the angle of attack.*

For a tailless aircraft configuration the determination of the neutral point location is the same problem as determining the aerodynamic center of the wing (when the fuselage influence is assumed to be small).

Assuming that the aerodynamic center is located in the plane of the wing, then one can write the pitching moment around the wing origin (leading edge of the wing root airfoil) as:

$$C_{Morigin} = C_{Mac_w} - (C_L \cdot cos(\alpha) + C_D \cdot sin(\alpha)) \cdot \frac{x_{ac}}{c_{ref}} \tag{4.5}$$

[1]Remember that the real point through which the aerodynamic forces act, is the point were there is no aerodynamic moment. This point is known as the center of pressure which changes location with the angle of attack

Rewriting Eq. 4.26 by ignoring the drag effects and assuming small angles of attack gives:

$$C_{Morigin} = C_{Mac_w} - C_L \cdot \frac{x_{ac}}{c_{ref}} \tag{4.6}$$

Differentiating this equation with respect to the angle of attack results in,

$$C_{Morigin,\alpha} = 0 - C_{L,\alpha} \cdot \frac{x_{ac}}{c_{ref}} \tag{4.7}$$

, which can then be written as

$$\xi_n = -\frac{C_{Morigin,\alpha}}{C_{L,\alpha}} \tag{4.8}$$

, in which c_{ref} is equal to c_{mac}.

4.3 Trimming a Tailless Aircraft

First one must understand the principles behind trimming a tailless aircraft. In a normal configuration the decalage angle of the horizontal tail is used to balance the moments, however a tailless aircraft is, by definition, lacking a horizontal tail surface. To trim this kind of aircraft one must make a distinction between swept and unswept wings. A zero sweep tailless aircraft, further referred to as flying plank, can not use the lift distribution, and thus not the twist, to change the moment coefficient around the aerodynamic center. It thus requires that the moment coefficient of airfoils is correctly chosen. To obtain a stable aircraft ($\sigma > 0$, center of gravity in front of the wing aerodynamic center) it is necessary to use airfoils with a slightly positive moment coefficient, around its aerodynamic center. Positive moment coefficient airfoils are in general less efficient than the others, so in order to achieve the best performance swept wing is needed.

$$C_{M_W} + C_{M_P} + \sum \left(\frac{dC_{M_W}}{d\delta} + \frac{dC_{M_P}}{d\delta} \right)_i \cdot \delta_i - C_L \cdot \sigma = 0 \tag{4.9}$$

If a flying wing aircraft is swept then the deflection of the elevator changes in general both the profile moment M_P and the wash-out[2] induced pitching

[2]Negative twist angle

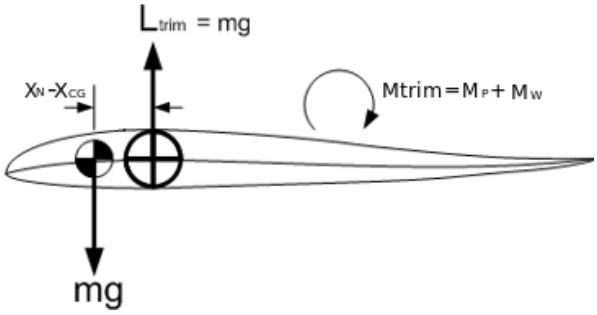

Figure 4.1: Forces and pitching moments acting on a tailless aircraft.

moment M_W, refer to Figure 4.1 and Eq. 4.30. Depending on the flap arrangement on the wing it may be possible that both moments have the same pressure effect or, that they are weakening each other. There are even configurations possible where there is no changes of balance with elevator deflection at all.

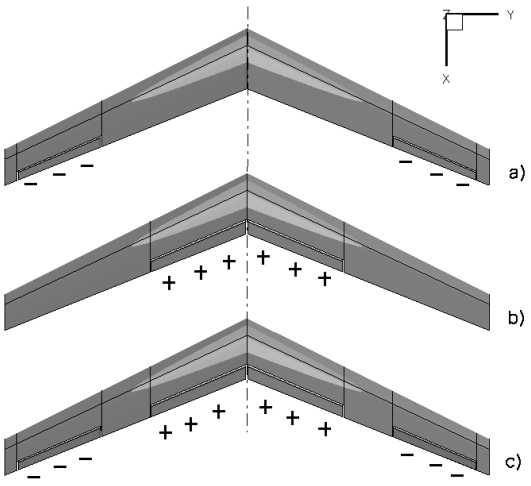

Figure 4.2: The possible arrangements of elevators on a sweptback flying wing. "+" means a flap deflection down, "-" a deflection up.

Fundamentally, there are three possible arrangements of elevators.

a) Outboard Elevators

Usually, on sweptback flying wings the designers prefer to put the elevators as far out as possible, refer to Figure 4.2 a) Thus they get the largest available distance to the cg, so an upward deflection increase the wash-out. This produces an additional positive moment M_W. Also, the profile moment M_P

is increased in the area of the elevators. Both moments have, thus, the same pressure sign and reinforce each other.

The wash-out induced pitching moment M_W increases approximately linearly with the sweep angles. This means, that for wings with a large sweep angle only small deflections of the elevator are needed. Hence the (still unavoidable) constriction of the flight polar becomes less and less severe with increasing sweep angle when comparing it with the flying plank.

The effectivity of the elevator, however, is not influenced much by an increase of the sweep angle. this stems from the fact that there are two different influences which largely cancel each other out : on the one hand for large sweep angle the elevator has also a large lever-arm and therefore a high turning moment. On the other hand, however, a wing with high sweep also has a large moment of inertia and therefore turns more slowly. Hence the pilot has more or less the same elevator control with a flying plank as with a highly swept flying wing.

b) Inboard Elevators

On a sweptback wing with high aspect ratio the elevators can also be arranged in the wing center, ref to Figure 4.2 b) By deflecting them downward the wash-out moment M_W of the wing is increased. The augmentation is proportional to the sweep angle. However, the profile moment M_P is diminished by that deflection. This is opposite to case a). Hence, the two pitching moments partially cancel each other out.

It depends upon the values of the sweep angle and the aspect ratio which one of these two moments outweights the other. If both the sweepback and the aspect ratio are very large then a down movement of the elevators rotates the aircraft nose up. This is corresponding to a canard-type airplane. In that case the sum of $M_P + M_W$ is positive (tail-heavy). If, in contrast, the sweepback and/or the aspect ratio is small then that sum can become negative. Then a downward elevator movement rotates the nose down.

c) Combination System

In Figure 4.2 c) the combination of the two system a) and b) is shown. It unites their advantages and avoids their disadvantages. It can be used if sweep angle and the aspect ratio are not too small.

In this system two control surfaces are used on either side. Each of them can stretch over one third of the half-span. The wing sweep should be so large that

the inner elevator "down" produces a tail-heavy moment. The control stick is then connected with the elevators in such a way that at "pull-up" the outer control surface rotates upward and the inner one down.

A primary advantage of this arrangement is that the wash-out (due to the flap deflections) is well-balanced over the wing. Furthermore the deflection angles needed are smaller than in case a) or b). Hence the angular differences between individual control surfaces are minimal.

Furthermore, this system is also quite favorable with respect to the influence on the laminar bucket : in the central wing area highest C_l values occur. There, at higher angles of attack the laminar bucket is shifted toward greater C_l values which is advantageous. In the middle part of each half-wing the profile is not altered. Hence, no deterioration occurs. Only in the outer parts of the wing is the laminar bucket shifted in the "wrong" direction. Because of the smaller deflection angles needed the situation is by no means as critical as with the other two variants a) and b).

The only disadvantage of this version - which really is very serious - is the increased construction requirement. Instead of only two control surfaces for a single control aircraft there are now four such surfaces needed. Therefore, this combination system is rarely used. In those cases where the augmented building requirement can be tolerated these additional inner surfaces are better utilized as (pitch moment free) landing flaps.

Chapter 5

Optimization Procedure

5.1 Optimization Algorithm

The objective function and some of the constraints applied to the optimization are non-linear and thus require a nonlinear optimization algorithm. Several algorithms are available to tackle these problems. However for this research the two algorithms of interest are the sequential quadratic programming algorithm, and the genetic algorithm. They are state of the art algorithms when dealing with complex optimization problems.

5.1.1 Algorithm Selection

The selection is based on their capabilities and limitations in handling the objective function and its constraints. An overview of both algorithms is presented to create a base for the selection process.

Sequential Quadratic Programming Algorithm

- Can get stuck in local minima;
- Able to handle strong nonlinear objective functions;
- Efficient use of objective function evaluations;
- Can handle all types of constraints (nonlinear, equality, inequality, bounds).

Genetic Algorithm

- Unlikely to get stuck in local minima, when the settings for the algorithm are correct;

- Able to handle strong nonlinear objective functions;
- Inefficient use of objective function evaluations;
- Can handle all types of constraints (nonlinear, equality, inequality, bounds).

From this overview it is clear that the differences are in the efficiency of the algorithm and the capability to handle local minima.

For a sequential quadratic program, the necessary and sufficient condition for a nonlinear minimization problem, is that the objective function and the constraints are convex. Determining the convexity of the objective function is impossible, as the objective function for performance optimizations, is dependent on many variables and the calculation of the aerodynamic forces is based on a numerical approach. The linear constraints are always convex but the nonlinear constraints are also dependent on the aerodynamic calculations imposing the same problem as for the objective function. The conclusion of this is that the use of sequential quadratic programming is not guaranteed to find a global minimum. So the genetic algorithm is used to find a global optimum.

5.2 Variables and Constraints

One of the first steps in setting up an optimization tool is to determine the variables. For the problem at hand two sets of variables are needed, geometric variables which define the wing geometry and variables that define the flow around the aircraft, like there are the velocity and the altitude. In this work the flow variables are all synthesized in the lift coefficient $C_L$that contain the indication of the altitude in the air density ρ and the flow velocity V_∞. After the definition of the variables it is important to recognize and define the linear and non-linear constraints.

5.2.1 Variables and Parameters

As already mentioned, there are two sets of parameters. The first set, the geometric parameters one, is used to unambiguously define the wing geometry. The assumption is made that the wing is symmetric with respect to the aircraft longitudinal plane, and the parameters thus define one side of the wing while the other side is mirrored. For simplicity in this thesis work the wings used for the simulations are constituted by a certain number of trapezoidal surfaces each one with its own geometric parameters, obviously the root and

tip sections of each surface have to be consistent with the dimensions of the nearby surfaces. The parameters to define a trapezoidal wing are:

- Section span, b;
- Quarter chord sweep, Λ;
- Taper ratio, λ;
- twist angle, γ;
- Surface , S.

Up until this point one parameter has not been discussed, namely the airfoil. At each wing section an airfoil has to be defined, however defining multiple airfoil options for each section causes discontinues jumps in the objective domain. These discontinues jumps in the domain will cause problems for the optimizer.

The only flow parameter, the lift coefficient, requires no further explanation, this is a single value defining the flight conditions. The geometric parameters and variables can be seen in Figure 5.1, 5.2 in which an example is presented of a wing with three sections (two surfaces). Most of the variables, to define the geometry for this example, will be vectors with two elements. All geometric variables require an upper and a lower bound and an initial value to start the optimization. The vectors of the bounds for the sweep and taper must have the same length as for the variables themselves such that different bounds can be applied to them for every section. The sum of all section spans will then be limited by these bounds. This is to enable the user to specify a total structural wing span. The "structural wing span" is intended to be the length of an hypothetical spar of the wing and not the distance between the root and the tip sections.

The initial values of the variables need to be provided. It is obvious that these initial values are contained within the specified bounds and that they preferably also meet the non-linear constraints. A good initial guess is not necessary but will most likely shorten the time it takes to find the optimum. The dihedral is not considered as a variable, as it mainly influences the lateral stability and not so much the range performance. This was the reason to only consider wings without dihedral. The airfoils have to be defined at all sections. The variables defined this far have been continuous variables, meaning that they can have any value within the constraints. The airfoils, however, are

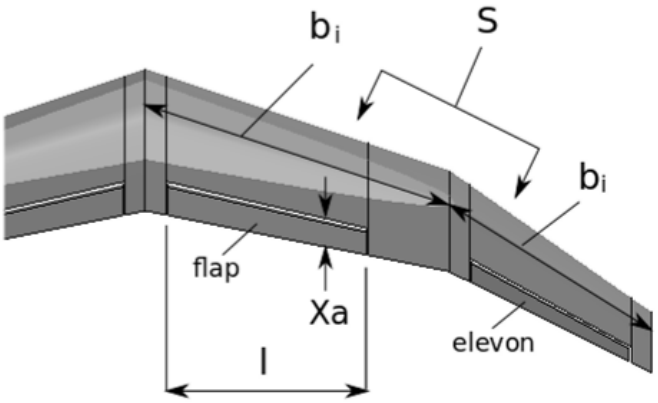

Figure 5.1: Configuration parameters.

implemented as discrete variables, which means that different options must be specified which all have to be evaluated separately. Having a lot of different airfoil combinations will increase the calculation time dramatically. The user has to provide all airfoil combinations that he/she wants to evaluate. Every airfoil combination then requires a separate optimization of the continuous variables. The best airfoil combination is selected at the end of all optimizations. This however is probably not the fastest way of optimizing and thus requires further investigation.

The panel method COMPA has been then submitted to an optimization algorithm that would be used to established the best wing shape for long range flight. The variables for the optimization would consist out of 3 geometric variables for each surface and 1 flow variable.

The 3 geometric variables are:

- the twist, γ;
- quarter chord sweep angle, Λ;
- the taper ratio,λ.

There are also "trimming variables" that consists in :

- α_i ith flight condition angle of attack;
- δ_i^j jthflap deflection angle of ith flight condition.

Apart from these variables several constant parameters are required. The most important ones are the total surface of the wing S, the wing span b

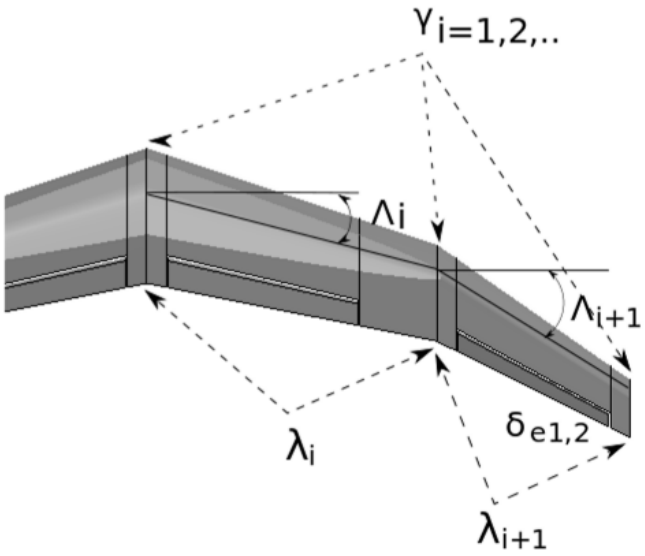

Figure 5.2: Configuration design variables.

and the stability margin m. The drag coefficient is taken as the objective for the optimizations presented in this thesis. The domain of the optimization variables was limited by linear and non-linear constraints. These constraints served the purpose to limit the search domain such that a valid design could be obtained.

5.2.2 Constraints

To limit the search field of the optimizer and to ensure a feasible design it is important to apply different kinds of constraints. A large distinction must be made between linear and non-linear constraints. In the wing optimization these two types of constraints will be used. The only linear constraints are inequality constraints. Is defined also a lower and upper bound for the variables. This type of constraints and the boundaries are embedded in the GA tool. The non-linear constraints serve the main purpose of providing a feasible design and ensuring the quality of the aerodynamic calculation. The non-linear constraints are enforced by appending penalty functions to the performance terms of the objective function, in order to reduce the computational effort needed when using the non-linear constraints GA's option.

All of the penalty functions implemented have the following form :

$$PF_i = K_p \left(d_i - d_o\right)^2$$

Where PF_i is the penalty function, d_o is the constrained value of the ith constraint, d_i is the actual value of the ith constraint, and $K_p$is the penalty weighting. This type of PF are chosen because are very simple and effective. Using K_p is possible to tune the PF adapting it to different type of constraints.

Penalty functions are used to enforce three types of constraints:

1. Static stability grater than a specified static margin $\sigma \geq m$;
2. Trim at specified flight conditions, $M_{CG} = 0$;
3. Specified flight conditions, $C_L = \overline{C}_L$.

5.3 Optimization Problem Formulation

All of aerodynamic shape optimization problems presented in this Thesis work, can be simplified to fall under the following model problem.

$$
\begin{aligned}
\text{minimize} \quad & C_D + PF_i \\
\text{with respect to these constraints} \quad & \gamma_i,\ \lambda_i,\ \Lambda_i,\ \delta_i^j,\ \alpha_i \\
\text{subject to these constraints} \quad & C_L = 0.2 - 1.0 \\
& \gamma_0 = 0^\circ \\
& S = const \\
& b = const \\
& m = 0.05 \cdot c_{mac} \\
& M_{CG} = 0 \\
\text{and to these boundaries} \quad & \gamma_{i,L} \leq \gamma_i \leq \gamma_{i,U} \\
& \lambda_{i,L} \leq \lambda_i \leq \lambda_{i,U} \\
& \Lambda_{i,L} \leq \Lambda_i \leq \Lambda_{i,U} \\
& \delta_{i,L}^j \leq \delta_i^j \leq \delta_{i,U}^j \\
& \alpha_L \leq \alpha \leq \alpha_U
\end{aligned}
$$

This model problem is then modified for each optimization, varying the number of variables and the values of the boundaries.

5.4 Calculation of Characteristics Points Positions

5.4.1 Calculation of Center of Gravity Position

The location of the center of gravity, X_{cg}, is determined using a simple model which assume a constant weight per unit surface area for the lifting surfaces and fixed weight for the payload.

5.4.2 Calculation of Neutral Point Position

As seen in Section 4.2 the calculation of Neutral point position involve the computation of two derivatives, they are generated using only two function evaluations for each derivative.

$$\frac{\partial C_{Mn}(\alpha)}{\partial \alpha} = \frac{C_{Mn}(\alpha + \Delta\alpha) - C_{Mn}(\alpha)}{\Delta\alpha}$$

$$\frac{\partial C_{Mcg}(\alpha)}{\partial \alpha} = \frac{C_{Mcg}(\alpha + \Delta\alpha) - C_{Mcg}(\alpha)}{\Delta\alpha}$$

This is possible because COMPA produces the aerodynamic coefficients using potential flow and so the dependency from angle of attack is linear. This imply that the moment coefficients derivatives are constant for the rage of angle of attack considered.

5.5 Mesh Convergence Study

Producing a "good mesh" is important to obtain good results. This, however, requires a lot of time and experience. Doing this automatically is rather difficult and does not ensure good meshes. The advantage of the mesh used by COMPA, is the fact that it is a surface mesh, meaning that only the surface of the wing needs to be meshed.

As said in the Chapter 2 the mesh generator can change the number of panels in chord and span direction in an easily.

This feature of MEG is used to perform a mesh convergence study to determine the number of panels in chord and span directions needed to obtain stable and precise results from the aerodynamic solver.

The convergence study is performed consider that what is important for the optimization is the drag coefficient, so the MCS has the aim of stabilize the C_D values during mesh refining.

This is performed implementing a cycle where, the mesh density is changed for every iteration and, using the angle of attack α as variable, the C_L is held constant, performing in this way a C_D which is dependent only by mesh thikness and not by C_L variation.

This consequently ensure that not only the C_D is well estimated but also C_L , due to the fact that exist a mathematical relation between the two coefficients.

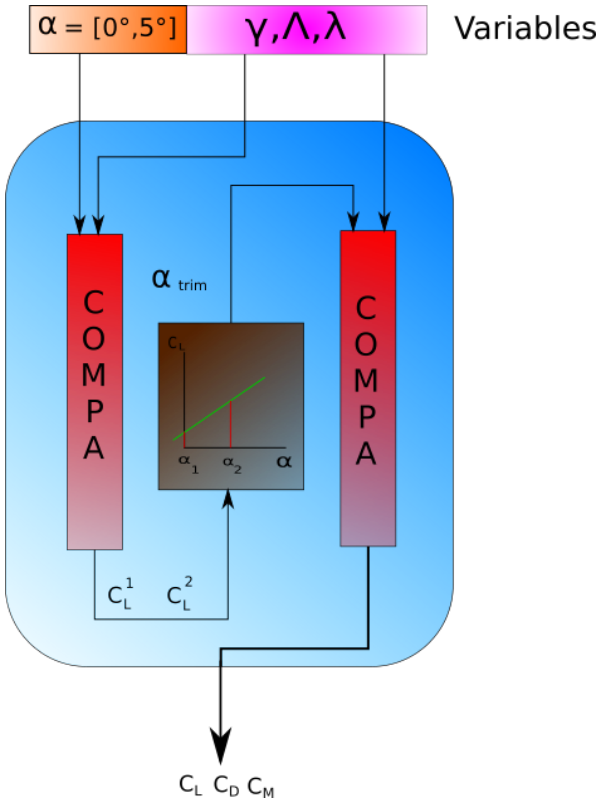

Figure 5.3: Flow chart of the mesh convergence study procedure.

It has been carried out a convergence study for each baseline geometry used in the simulations. This is because every geometry has its particular needs for what concern mesh density.

The MCS results are presented in Sections 6.4, 7.1.3, 7.2.3, 7.3.3 for what concern section 6.4 a complete description of the results is presented using graphs and numbers. In Section 7.2.3, 7.3.3, only a table with five values is reported.

The values reported in the table 7.3 7.6 are obtained from a sampling of the surface that represent the trend of aerodynamic coefficients changing N_{chord} and $N_{wingspan}$. The samplings are made following the steepest descent direction.

5.6 Program Set-Up

In this section are reported some technical aspects concerning OT and in particular are discussed the termination criteria which are fundamentals in order to catch the optimal solution without wasting time in usefulness iterations.

The working flow chart in Figure 5.4 shows the links between the main parts of the OT, it looks like very simple and "linear", but what the flow chart doesn't show is the complicated and many times unintuitive tuning of the parameters which is behind each OT part.

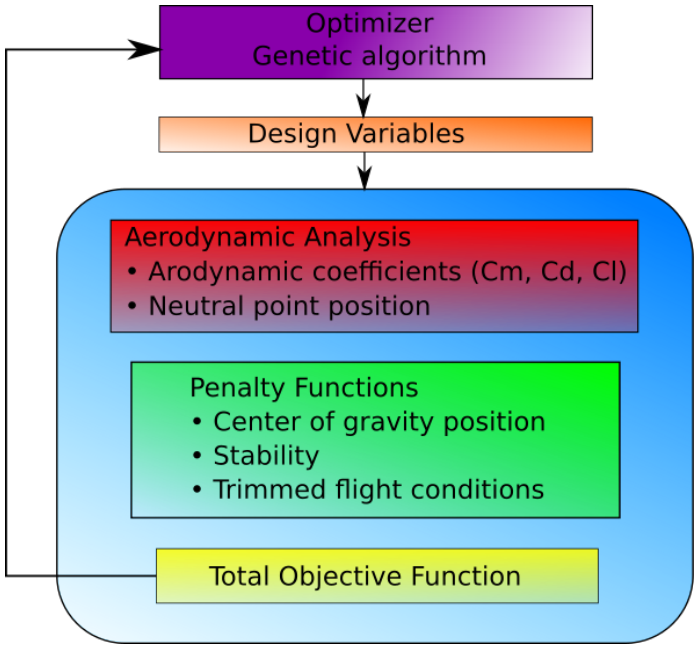

Figure 5.4: Flow chart of the working procedure.

5.6.1 Program Initialization

The program initialization serves the purpose to provide the information needed by the program to start the optimization. Several inputs are required to define some constant design values and to define the boundaries and initial values of the optimization variables. An overview of these parameters can be found below.

Fixed Parameters

The fixed parameters are used to define some specific wing details, that are constant during the optimization.

- General parameters
  - Lift coefficient;
  - Stability margin [%];
  - Numbers of mesh panels in chord and span direction.
- Wing geometric parameters
  - Total Surface $[m^2]$;
  - Total structural wing span $[m]$;
  - NACA airfoil for each control section [NACA four digits];
  - Flaps distribution along wing-span;
  - Flaps chord [% of wing chord];
  - Variable boundaries.

What is very important to set with care, are the boundaries of the trimming variables $\left(\alpha_1, \alpha_2, \delta_1^j, \delta_2^j\right)$, in fact the aerodynamic solver used COMPA is linear inviscid, so do not consider flow separation. This imply that if the ailerons deflection overtake a certain value, COMPA is not able to catch the correct phenomena and so comes out with inaccurate aerodynamic coefficients. This problem occur also with angle of attack, if it is too close to wing stall region, the non-linearities degrade the quality of results.

To have an idea of the boundaries, is possible to use the (C_L, α) diagrams concerning the NACA airfoils used. From these graphs the boundaries are extract considering the region where the airfoil features are linear. Refer to Figure 5.5 for an example.

5.6.2 Evaluating the Objective Function

Once the optimization is initialized, the iterative loop of looking for the best wing can be entered. The first step in this loop is to build up the first generation that respect the imposed linear constraints. In fact, using as optimizer a GA, it needs a certain number of individuals in order to start optimization loop. Then at each individual of first generation is applied a certain *score,* this *scores* are calculated evaluating for each individuals the objective function. It comprehends the real index of merit that is the *Drag coefficient* C_D and the penalty functions that ensure the constraints respect.

Consider the facts that : **optimization is single objective**, it has to be performed considering trimmed horizontal leveled flight and which the drag is

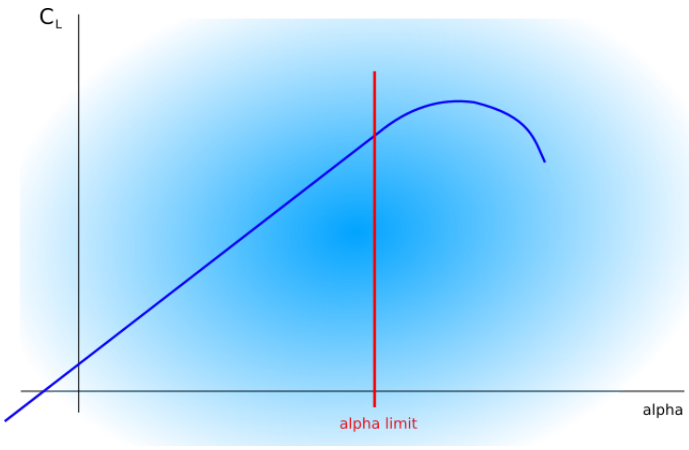

Figure 5.5: Angle of attack boundary.

evaluated at two flight conditions corresponding to high speed glide $C_L = 0.2$ and low speed thermaling flight condition $C_L = 1$.

Taking into account what said above, the objective function is composed evaluating each individuals at the two flight conditions,the drag is calculated consider trimmed flight together with the penalty functions effects, refer to Figure 5.6. The trimming is ensured consider as variables the angles of attack α_i and the flaps deflection angles δ_j^i for the two flight conditions.

When the objective function is evaluated, as seen above, for each individual of first generation, a vector of *scores* is available. Using this *scores* the GA choose the best one and starts to build up the new generation. This procedure continues until termination criteria are not involved.

5.6.3 Checking Termination Criteria

Once the optimization is running, it must know when it is close enough to the optimum to stop. This is done by the termination criteria. There are two types of termination criteria, the once that limit the number of iterations or function evaluations and the ones that put constraints on the variation of certain values. The limitations on the number of iterations and function evaluations are set such that they are almost never the termination criteria. This is because they can stop the optimization before the actual optimum is found. However they become active in case the optimization is taking to long or a optimum is hard to find. The other criteria take into account the variation of the objective function, the variation of the variables and the tolerance on the non-linear constraint violation. Ones these criteria are met the optimization will break out of the iterative loop and assume that the obtained result is the optimum.

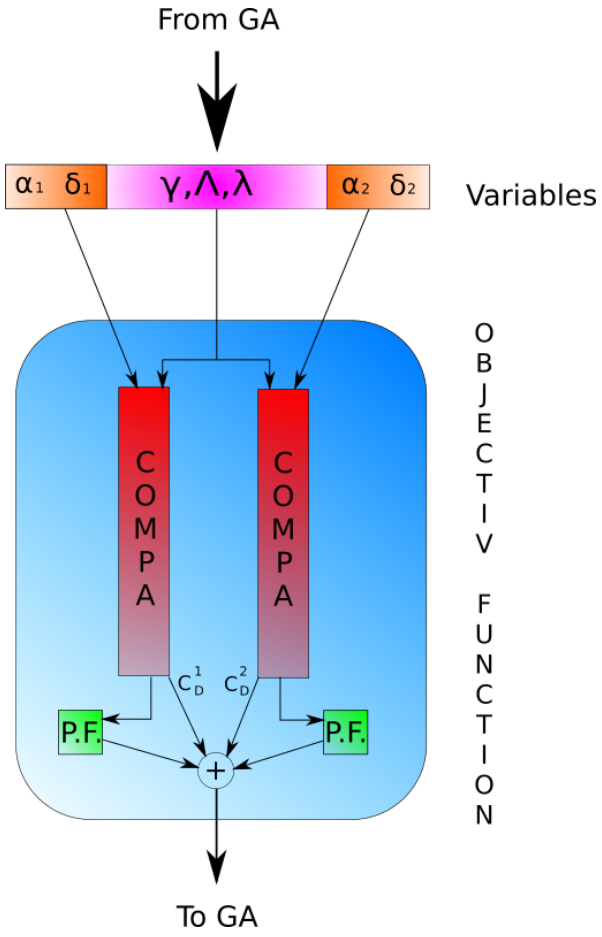

Figure 5.6: Flow chart of the objective function evaluation .

Chapter 6

Validation

6.1 Introduction

An important aspect in the optimization tool development is for sure the validation. A way to validate a numerical procedure is to choose a minimization problem that has theoretical solution and compare theoretical results with numerical ones. From the comparison, it is possible to evaluate if the OT is capable of reproducing theoretical results and so judge if the optimization problem is well-set and if all the parts which compose the OT work correctly. It is also possible to get sensibility informations. The validation could also be a way to understand the optimization procedure weaknesses and manage them in order to improve the quality of the results.

6.2 Problem Definition

In order to validate the optimization cycle is possible to take as theoretical result the fact that to minimize the induced drag of a wing, the optimal span wise C_l distribution is elliptic.

This fact is true, consider total produced lift and wingspan fixed during the optimization procedure.

The ways to manage the C_l distribution are mostly two : modify the chord of wing sections in different span positions or change the geometric twist of the sections, whereas aerodynamic twist changes lift by using different airfoil sections along the span. The best way to approximate an elliptic distribution using the methods explained above, would be to discretize the wing in an infinite number of sections. This is obviously impossible, so the number of

sections used in the simulation is 5 for every half wing. This number has been chosen in order to achieve a good compromise between nice results in terms of discretization and computational effort.

The problem of keep constant the total lift produced, could be solved consider a wing with fixed surface and imposing as optimization constraint a certain C_L. In order to have a wing with fixed surface the "geometric twist method" has been used. The "geometric twist method" is referred to the way with the C_l distribution is modified.

In this way the constraints are observed and the optimizer can work with a well posed problem using as optimization variables the twist angles of the sections.

Summarizing, the goal of this optimization case is to perform lift-constrained drag minimization of a rectangular wing using OT implemented in this thesis work.

6.3 Baseline Geometry

Rectangular wing without flaps and with symmetric airfoils NACA 0011, refer to Figure 6.1.

$AR = \frac{b^2}{S} = 8$

About the geometry a very important aspect is the mesh distribution. In fact the choice of the proper number of elements along wingspan and chord direction is the key to obtain good and stable results.

The control sections used in the optimization are equally spaced along the wingspan.

6.4 Mesh Convergence Results

The upper image in Figure 6.2 quickly put out the region where C_D became less sensitive to mesh variation. The lower image is the contour representation of the upper one, the arrows visible on the contour, represents the gradient of the surface. Where the gradient is practically null, it is possible to assume that the aerodynamic solution is not affected by mesh distribution. On z axis is put the percentage error calculated considering as reference value the coefficient computed with the maximum number of mesh elements. In fact in general more dense is the mesh more accurate are the aerodynamic coefficients computed with it.

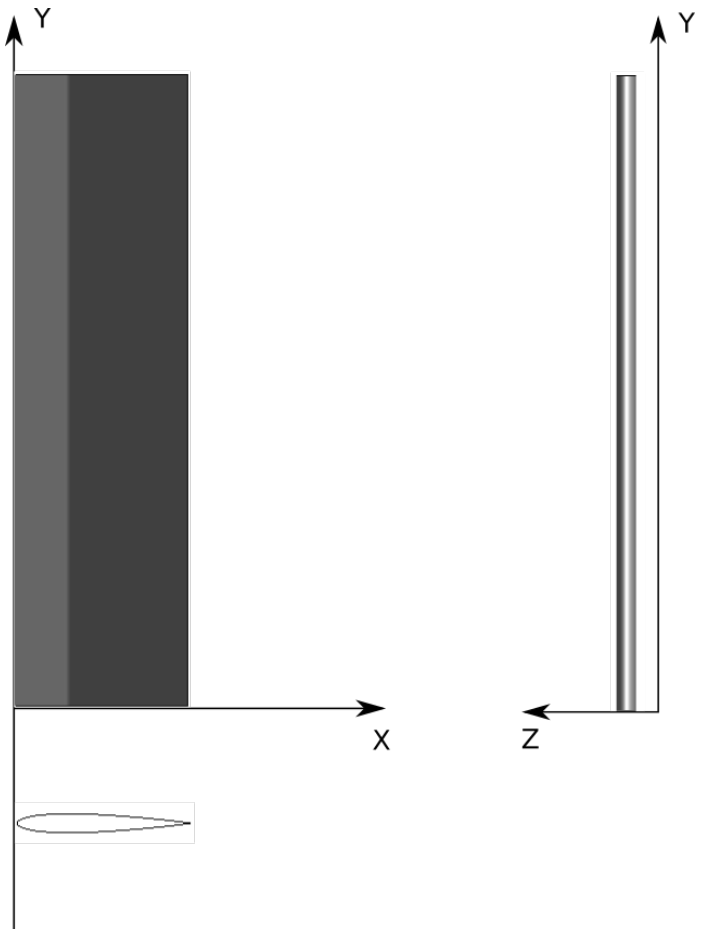

Figure 6.1: Baseline geometry.

As it is possible to see from the images of Figure 6.2 there is a region where the variation of aerodynamic coefficients due to variation of panel distribution is minimum, the number of panels in that region is the correct choice to have the best results with the minimum computational effort.

Point N.	Mesh Size	N_{chord}	$N_{wingspan}$	C_D	C_L	$\alpha[^\circ]$
M1	1500	100	15	0.0042	0.25	3.22
M2	6500	100	65	0.0044	0.25	2.99
M3	300	20	15	0.0056	0.25	3.21
M4	1300	20	65	0.0057	0.25	3.03
M5	2700	90	30	0.0043	0.25	3.12

Table 6.1: Mesh convergence study results.

In the table are reported some significant points of the domain that show the trend of coefficients varying the mesh thickness.

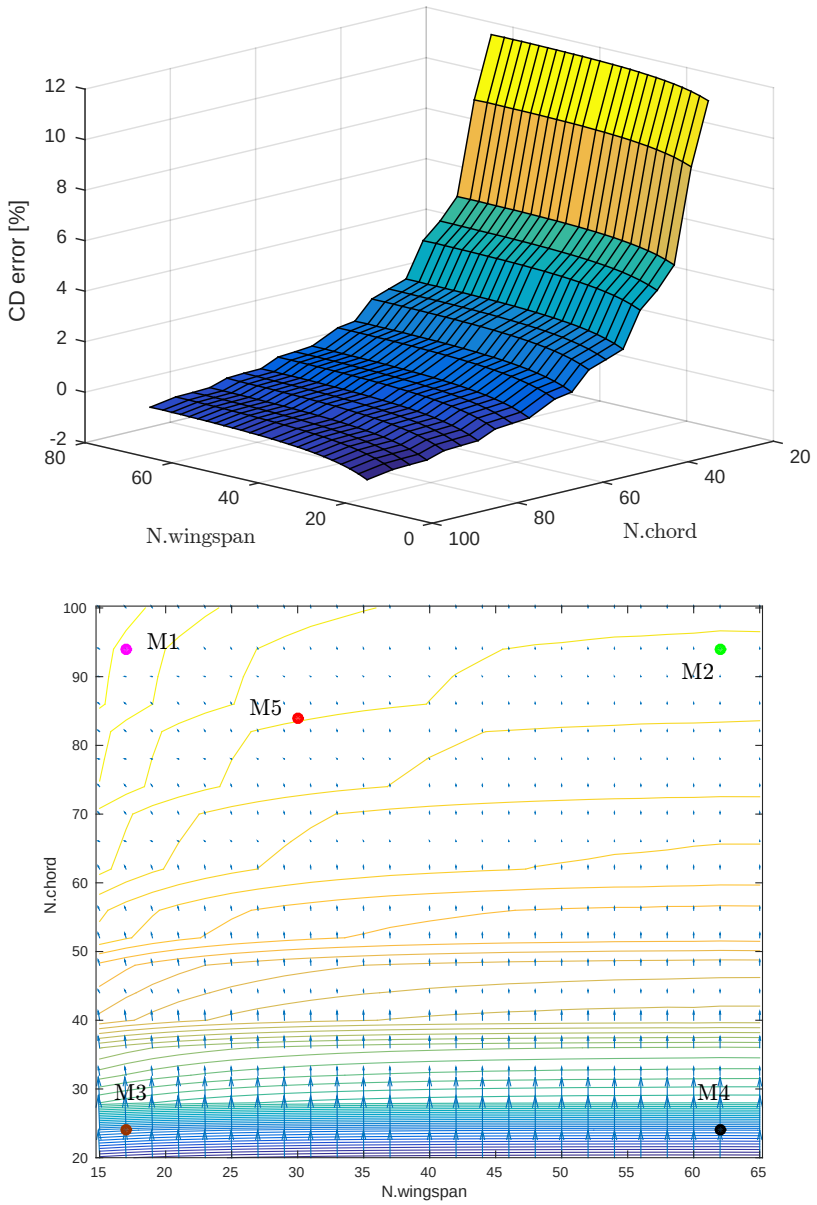

Figure 6.2: Graphics representation of mesh convergence study.

The number of panels and the mesh size are referred to a semi-wing.

Below are reported the numbers of panels in chord and span direction used in this simulation. They correspond to point M5

$N_{chord} = 90$

$N_{wingspan} = 30$

From the data reported in Table 6.1 and also in Figure 6.2 is clear how the C_D variation is bigger in N_{chord} direction. In fact using less than half panels

respect to point M2 but having almost the same N_{chord} the two C_D are very close to each other.

6.5 Optimization Problem Formulation

The aerodynamic shape optimization seeks to minimize the drag coefficient by varying the shape design variables subject to lift constraints $C_L = 0.2, 1.0$.

The shape design variables are the twist angles of 5 control sections equi-spaced between root and tip including tip section and the angle of attack.

Initial population is chosen randomly by genetic algorithm procedure with an imposed number of individuals of 60.

The complete optimization problem is described in Table 6.2.

	Function/variable	Description	Quantity
minimize	$C_D + PF_i$	Drag coefficient + Penalty function	
with respect to	α	Angle of attack	1
	γ_i	Twist angles	5
		Total design variables	5
subject to these constraints	$C_L^1 = 0.2$	Lift coefficient 1^{st}simulation	1
	$C_L^2 = 1$	Lift coefficient 2^{nd}simulation	1
	$\gamma_0 = 0^\circ$	Root section's twist angle	1
	$S = const$	Surface	1
	$b = const$	Structural wingspan	1
		Total constraints	4
and with these boundaries	$-7 \leq \gamma_{1,2,3,4} \leq 0$	Twist angles	/
	$0 \leq \alpha \leq 18$	Angle of attack	/
with this starting point	$\gamma_1^i, \gamma_2^i, \gamma_3^i, \gamma_4^i, \gamma_5^i$	Twist angle initial population	60×5
	α^i	Angle of attack initial population	60
	$\gamma_1^i, \gamma_2^i, \gamma_3^i, \gamma_4^i, \gamma_5^i + \alpha^i$	Individual	
		Total initial individuals	60

Table 6.2: Schematic descripion of the optimization problem.

The constraints on C_L are imposed using a penalty function. In particular the P.F. used have the formula and shape shown below.

$$PF_i = K_p \left(d_i - d_o\right)^2$$

	PF_1	PF_2
K_p	100000	100000
d_o	0.2	1

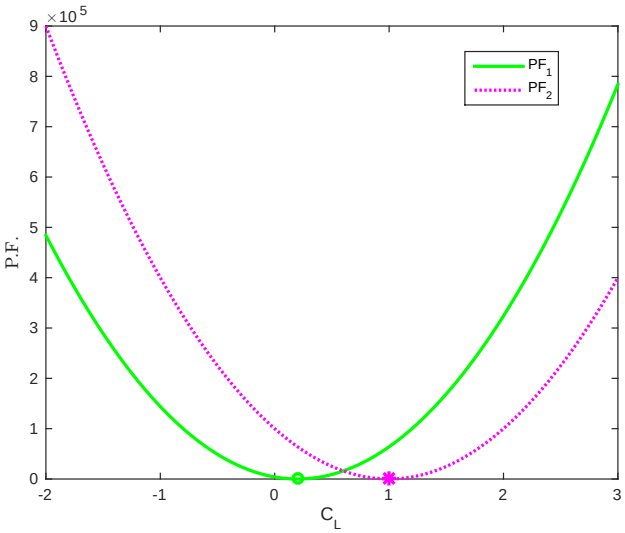

Figure 6.3: Penalty function used to impose $C_L = 0.2, 1$.

6.6 Results and Comments

As seen above the tests have been performed imposing C_L 0.2 and 1.0. This is because the aim of the test was to validate the OT for the "real work conditions". In fact the purpose of the tool is to optimize a flying wing for a range of flight conditions, so here are taken the boundaries of flight envelop to be sure that the OT work well in all conditions.

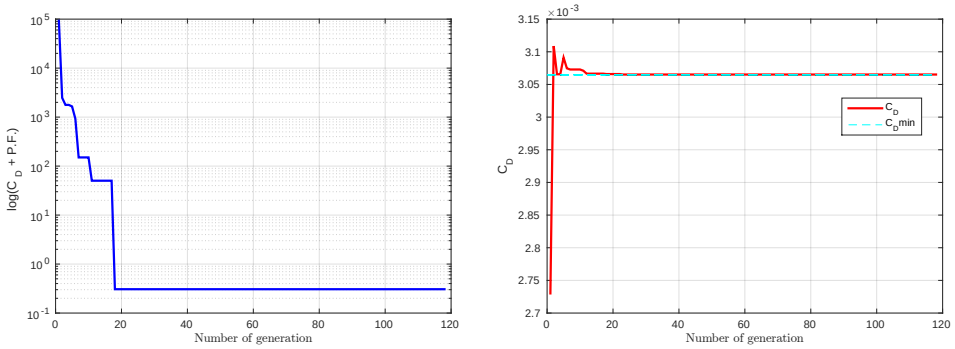

Figure 6.4: Objective function and drag coefficient trend during optimization with $C_L = 0.2$.

Looking at the red graphs of Figures 6.4 and 6.5 is possible to notice how for both the tests the C_D trend during optimization looks like opposite to the correct direction, it grows up instead of decreasing. The explanation is that the optimization is bounded to obtain a certain C_L, so if the starting individual has a C_L smaller than the target one the C_D has to increase. What

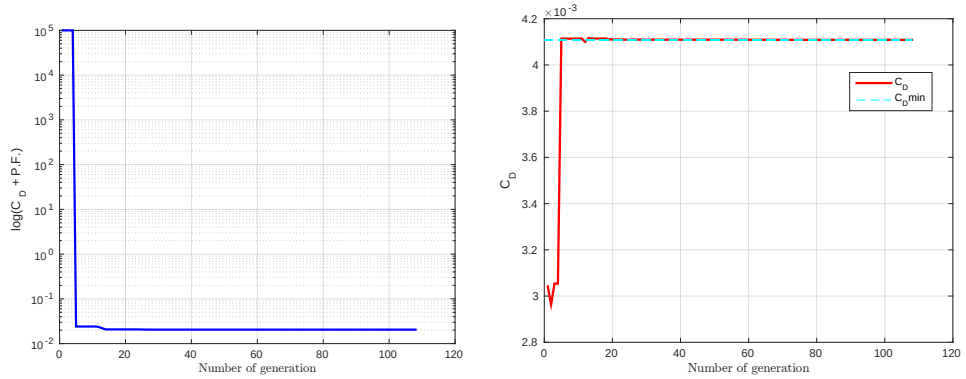

Figure 6.5: Objective function and drag coefficient trend during optimization with $C_L = 1$.

is important to notice is that after a certain number of generations the C_D value is kept constant.

What is meaningful to observe in order to understand if the optimization has worked or not is the objective function trend. Blue graphs of Figures 6.4 and 6.5 show that in both the tests the objective function decrease monotonically, starting from a huge value, drop down quickly and stabilizing for the rest of the generations. The starting huge values are due to penalty function presence, which penalize the individuals that not respect the constraints.

The flat part of the graphs represents a typical behavior of GA, in fact it works producing one or more drops in the fitness function. When the stable part comprehends a big number of generations it means that the GA is stuck in a global minimum.

Figures 6.6 and 6.7 show a detailed comparison of the first best individual and the optimized one. In these Figures, the FBEI features are shown in red and the optimized wing features are shown in blue. At the optimum, the lift coefficient target is met. The lift distribution of the optimized wing is much closer to the elliptical distribution than that of the FBEI, indicating an induced drag that is close to the theoretical minimum for a planar wake. This is achieved by fine-tuning the twist distribution.

The optimized twist distribution of the first test is significantly different from that of the baseline, as is possible to see in Figure 6.6 and Table 6.3, the optimizer redistributed the twist in order to fill up the lack of lift in the middle part of FBEI. For what concern the second test, the baseline and optimized twist distributions are very similar to each other, what is pretty different is the angle of attack that in FBEI is too small.

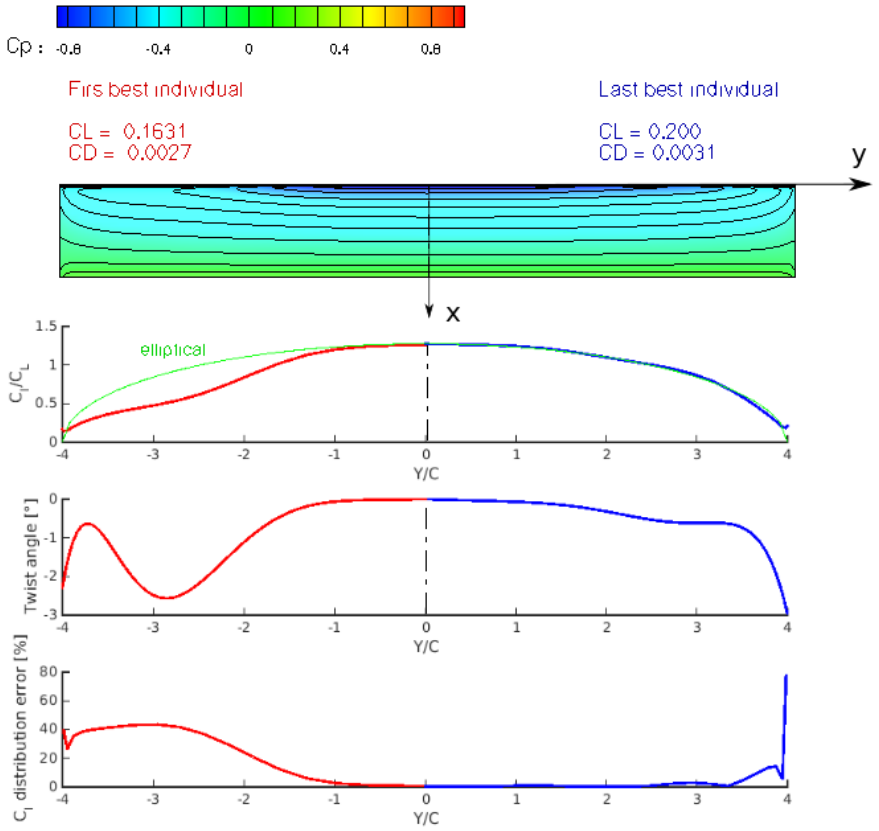

Figure 6.6: Comparison between C_l distribution of first generation best individual (on the left) and the last generation best individual (on the right) with $C_L = 0.2$.

		$\gamma_{root} \rightarrow \gamma_{tip}$					
First best individual	γ	0°	-0.0315°	-0.4480°	-1.9904°	-2.0915°	-2.2928°
	Y/c	0	0.8	1.6	2.4	3.2	4.0
	C_L	0.1631					
	C_D	0.0027					
	α	2.92°					
Last best individual	γ	0°	-0.0512°	-0.1731°	-0.4940°	-0.6109°	-2.9463°
	Y/c	0	0.8	1.6	2.4	3.2	4.0
	C_L	0.2000					
	C_D	0.0031					
	α	2.74°					

Table 6.3: Results of the test with $C_L = 0.2$.

6.7 Effect of the Number of Control Section

The cost of computing a generation with a GA is nearly independent of the number of design variables, it is dependent by the number of items that com-

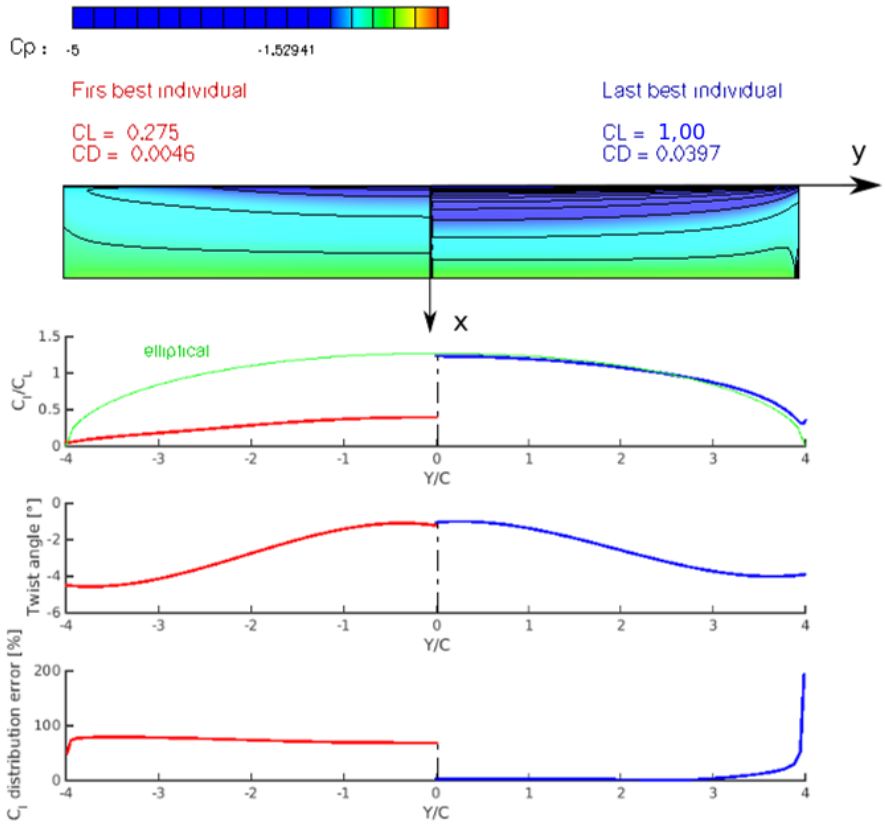

Figure 6.7: Comparison between C_l distribution of first generation best individual (on the left) and the last generation best individual (on the right) with $C_L = 1.0$.

		$\gamma_{root} \rightarrow \gamma_{tip}$					
First best individual	γ	0°	-0.827°	-1.2226°	-1.7805°	-3.7308°	-4.4896°
	Y/c	0	0.8	1.6	2.4	3.2	4
	C_L	0.2702					
	C_D	0.0053					
	α	5.8217°					
Last best individual	γ	0°	-0.532°	-1.0507°	-1.7175°	-3.3991°	-3.8947°
	Y/c	0	0.8	1.6	2.4	3.2	4
	C_L	1.0019					
	C_D	0.0380					
	α	14.4404°					

Table 6.4: Results of the test with $C_L = 1$.

pose the generation. The problem is that the number of items is driven by the number of design variables following a certain proportionality. For example in this thesis work a proportionality of 10 is used, it means that for each design variable must be added 10 individuals.

Can be interesting to determine the trade-off between the number of design variables and the optimal drag coefficient, and to examine the effect on the computational cost of the optimization. Thus, in this section the effect of reducing the number of design variables is analyzed.

Optimization problems of this section are performed using the M5 mesh grid with variations in the number of control sections. Figure 6.8 shows the resulting optimized designs for different numbers of airfoil control sections.

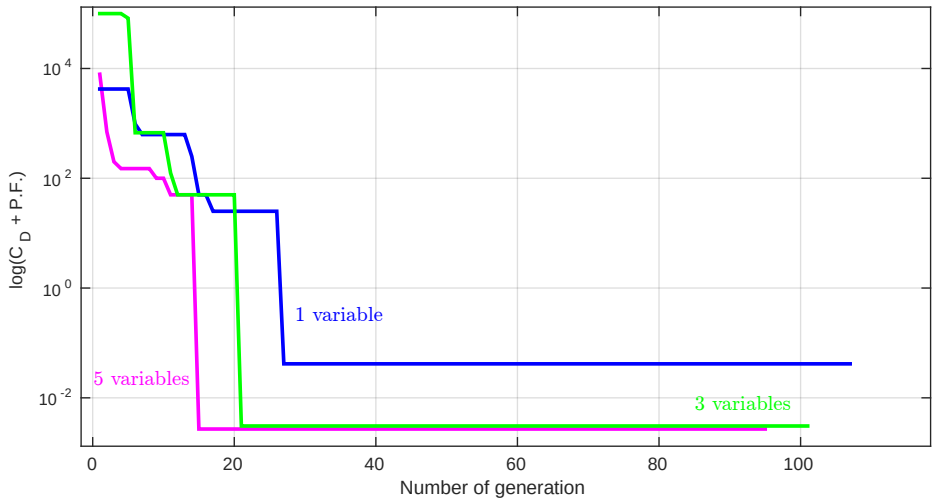

Figure 6.8: Objective functions trends during optimization.

The number of variables indicated in the figure include only the number of control sections used in the optimizations, the angle of attack is excluded. The number of control section is always referred to an half-wing.

The Figure 6.8, shows that decreasing the number of variables, the optimized objective function became bigger. This could be caused by the fact that less control sections means reducing in a certain way the discretization of the wing in spanwise direction, and so reduce the OT capability of carfully follow the elliptical C_l distribution.

Reducing the number of variables has a negligible effect on number of iterations, this is not true if we look at computational time. In fact remembering what said about the relation[1] between number of variables and number of items in a generation, it is possible to affirm that with three variables the computational time is reduced and the optimality of the result is not so compromised.

[1]The relation used in this Thesis work is 10 individuals for one variable.

From this study it is possible to conclude that an adequate optimized design can be achieved with a smaller number of design variables.

6.8 Conclusion

The results shown above tell us that the optimization problem is well-set and the OT is able to find global minima respect to some constraints. Also the penalty functions set-up seem to be pretty well suited for this type of optimization, in fact the objective functions trends during optimization are thrilling descents that take the C_L value to perfectly match the constrained one.

Obviously this results are indicative and do not give the sureness that the OT works perfectly in any other condition. The validation test says that with the correct set-up OT is able to catch the exact solution compared with theoretical results.

Chapter 7

Application Studies

In this chapter the results obtained with the OT will be discussed and analyzed. Firstly a preliminary study has been performed, this consist in a series of optimizations each one with a parameter or a variable fixed at a certain value. This allows to plot different graphs which help to becoming familiar with the solutions space. Then two different optimizations were performed to investigate different parameters set-up, in order to understand how the parameters affect the performances of the wing. The first of these optimizations were used to establish the best possible wing assuming to have a simple trapezoidal wing. For the second optimization the baseline wing is composed by two trapezoidal parts in order to see how much could be gained increasing the number of optimization degrees of freedom.

The initial populations are built up in order to respect the variables boundaries but are completely independent from non linear constraints. The initial populations could not comply the constraints, in fact non linear constraints are imposed using PF.

7.1 Preliminary Studies

7.1.1 Problem Description

In this section the results of many optimizations are presented together using different graphs. This has the purpose of inspect how the solution space is composed and have an idea of the performance sensibility to variables changes.

This help to better understand how to tune the various OT parameters and became familiar with its features.

7.1.2 Baseline Geometry

Simple trapezoidal wing with flap and with symmetric airfoils refer to Figure 7.1

Wing Parameters :

- Symmetric airfoils NACA 0012;
- One flaps for half-wing;
- Flaps position and length (Referring to Figure 2.10 for the symbols);
  - $s = (55)$ [% of b];
  - $l = (35)$ [% of b].
- Flaps chord 20 [% of wing local chord].

The control sections used in the optimization are the root and tip section.

7.1.3 Mesh Convergence Study

Aerodynamic shape optimization is a computational intensive endeavor, where the majority of the computational effort is spent in the flow solution. In particular computational effort is high when the aerodynamic mesh is dense and decreases if the size of the mesh is reduced.

Mesh Size	C.T. [s]
2800	13
5500	65

Table 7.1: Computational time comparation. The time is referred to a single aerodynamic simulation.

In this section there are graphs composed by results of many simulations which need very much time to be computed. Is also important to say that what is substantial in this graphs are the trends of the variable and not the exact values.

This consideration is used to reduce the computational time needed to produce the results of this section just using a coarser mesh with respect to the one used in sec 7.2, 7.3.

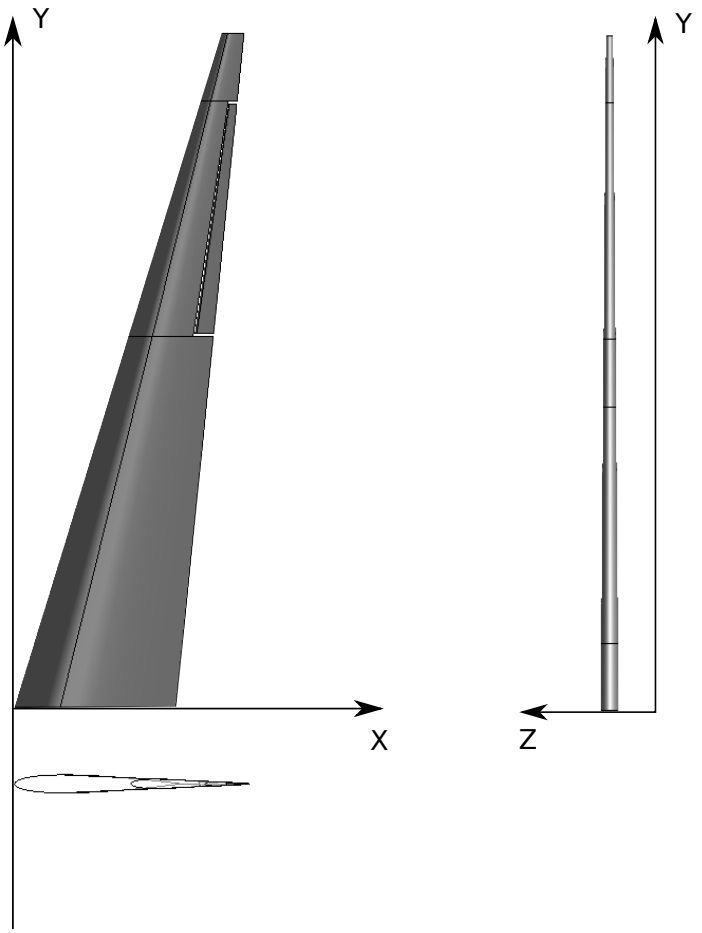

Figure 7.1: Baseline geometry.

Obviously this procedure can be consider valid if the coarser mesh produces results that probably are not exact from magnitude point of view, but they have to show the same trends of results obtained with a finer mesh.

This fact has been verified conducting a grid convergence study of the optimized design.

The variation in drag coefficient between the baseline and optimized meshes is nearly constant for each grid level refer to Figure 7.2, which gives confidence that the optimizations performed with the coarser meshes produce results having the same trends of those produced with a finer mesh .

In this case the MCS is performed considering a fixed ratio between N_{chord} and $N_{wingspan}$, this is the reason why the plot is a 2D figure and are reported only the total number of elements that compose the mesh. This ratio is fixed to be $\frac{N_{chord}}{N_{wingspan}} = 1.4$.

In the figure 7.2 are reported the results for a single point optimization with

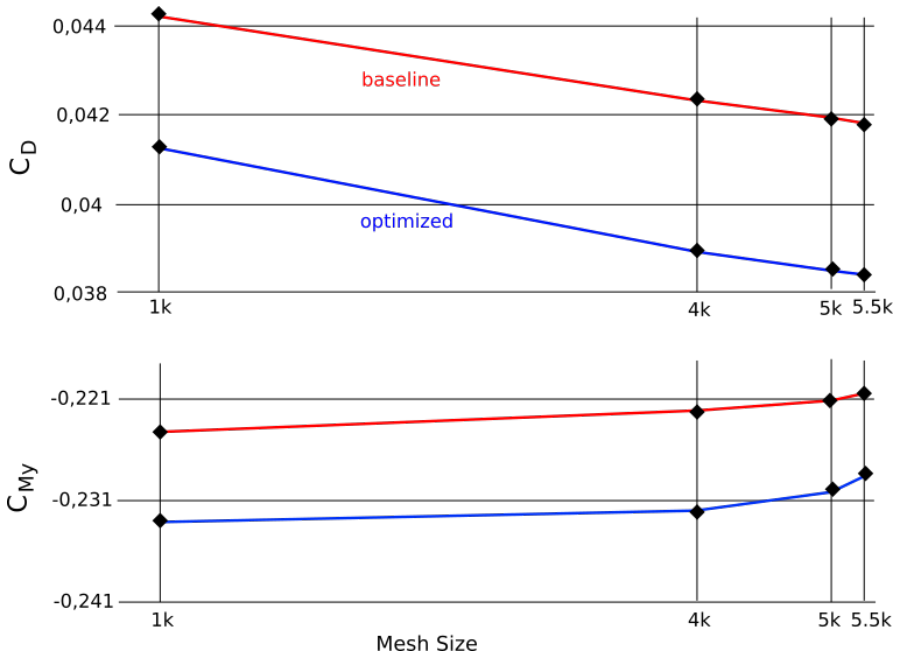

Figure 7.2: Mesh convergence graph for both the baseline and optimized geometry meshes.

an imposed C_L of 1.

7.1.4 Optimization Problem Formulation

The results presented in this section are obtained performing many different optimizations, these aerodynamic shape optimization seeks to minimize the drag coefficient by varying the shape design variables, the optimization is subjected to several constraints, the most important are :

- Lift coefficient $C_L = 0.2, 1.0$;
- Stati margin $m = \overline{m}$
- Trim $M_{CG} = 0$.

The shape design variables are twist angle of root and tip section, taper ratio, sweep angle and the trimming variables : angle of attack and flap deflection.

In the different optimizations one parameter at a time is kept fixed, the wing is optimized and the results saved. Then the value of the fixed parameter is changed and another optimization is performed, the procedure is repeated for each variable you want to analyze.

Initial population has been chosen using a code that use random proceses to generate the individuals, This help to increment the convergence velocity.

The complete optimization problem is described in Table 7.2. The Quantities reported in the table are referred to only half-wing.

	Function/variable	Description	Quantity
minimize	$C_D + PF_i$	Drag coefficient + Penalty functions	
with respect to	γ_1	Twist angle	1
	λ	Sweep angles	1
	Λ	Taper ratio	1
	δ	Flaps deflection	1
	α	Angle of attack	1
		Total design variables	5
subject to these constraints	$C_L = 0,2 - 1$	Lift coefficient	1
	$\gamma_0 = 0°$	Root section's twist angle	1
	$S = const$	Surface	1
	$b = const$	Structural wingspan	1
	$m = 0.05 \cdot c_{mac}$	Static margin	1
	$M_{CG} = 0$	Static equilibrium	1
		Total constraints	6
and with these boundaries	$-7 \leq \gamma_1 \leq 0$	Twist angles	/
	$0 \leq \lambda \leq 40$	Sweep angle	/
	$1 \leq \Lambda \leq 8$	Taper ratio	/
	$-10 \leq \delta_i^j \leq 10$	Flaps deflections	/
	$0 \leq \alpha \leq 18$	Angle of attack	/
with this starting point	$\gamma_{1,2}^i, \lambda_{1,2}^i, \Lambda_{1,2}^i, (\delta_1^{1,2})^i,$ $, (\delta_2^{1,2})^i, \alpha_1^i, \alpha_2^i$	Individuals	70

Table 7.2: Schematic descripion of the optimization problem.

7.1.5 Results and Comments

The results presented have the intent to show the most relevant trends for each variable used as parameter in the different optimizations, plus the results about static margin which is an important parameter to define the wing features.

In order avoid confusion, here it is declared the sign convention used for twist angle and flap deflection.

- Twist angle is positive when the airfoil trailing edge is moved down;

- Flap deflection angle is positive when the aileron trailing adge is moved up.

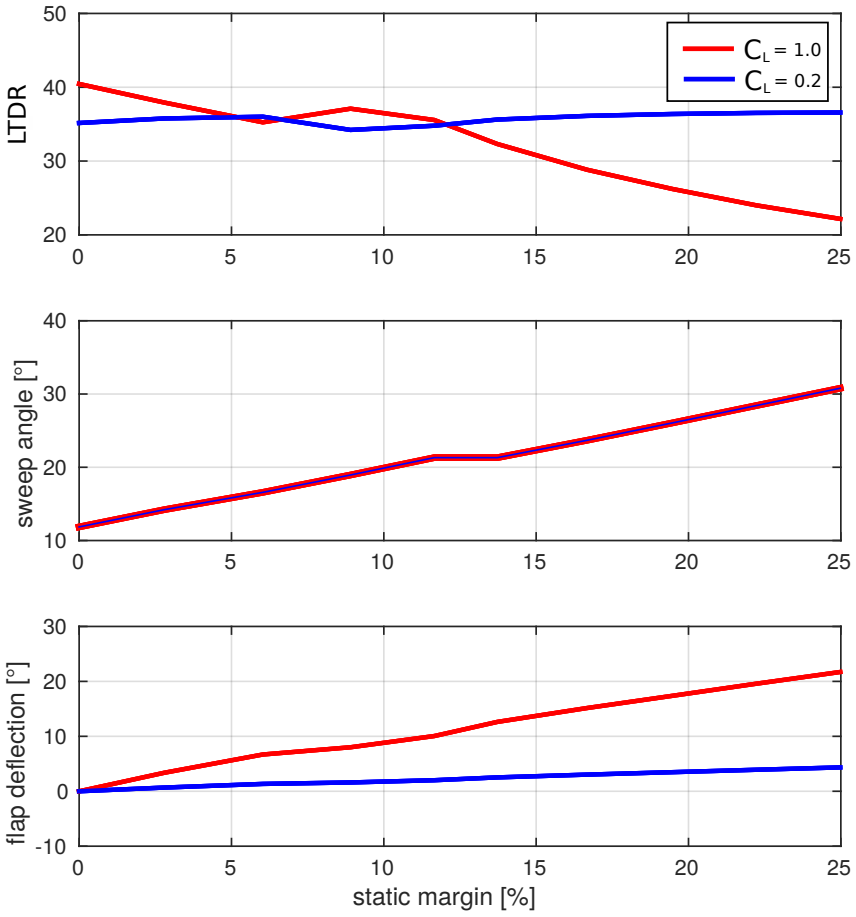

Figure 7.3: Optimal values for lift-to-drag ratio, sweep angle and flap deflection angle as a function of static margin.

Referring to Figure 7.3, the top graph show the LTDR trends as function of the static margin, for what concern the flight condition with $C_L = 1$, it decrease incrementing the static margin. This behaviour is understandable considering that, an increase of the static margin imply a growth of the sweep angle and so an AR reduction that increase the induced drag reducing the LTDR. About flight condition with $C_L = 0.2$, it is more difficult to interpret, the LTDR is more or less constant, tend to increase slightly, increasing the sweep angle. A possible explanation could be formulated considering that with low C_L the relative importance of the induced drag on total C_D is less relevant, so the

reduction of frontal section area due to the sweep angle increase, produce a pressure drag reduction which is bigger with respect the induced drag increase. This imply a slightly increment of the LTDR.

For what concern the sweep angle the two flight conditions have practically the same trend, the reason is that the neutral point and center of gravity positions are function only of the wing geometry and not of the flight condition.

The flap deflection increase if the static margin increase, in fact the neutral point position move back towards wing trailing edge requiring a bigger trim torque and so a bigger deflection.

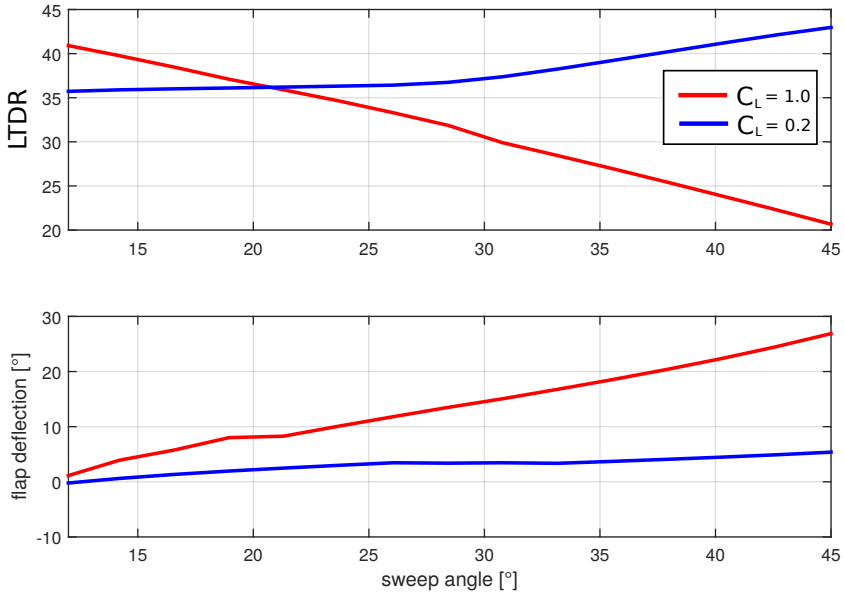

Figure 7.4: Optimal values for lift-to-drag ratio and flap deflection angle as a function of sweep angle

Referring to Figure 7.4, the LTDR behaviour has the same motivations explained before, in fact the static margin and sweep angle are proportional to each other.

The sweep angle starts from the value of 12° because with a less angle the wing is unstable with a negative static margin. It is clear also looking at the second graph of Figure 7.3

Also the flap deflection trend is very similar to which of Figure 7.3.

The graphs shown in Figures 7.5 and 7.6 are obtained considering a static margin of 7%.

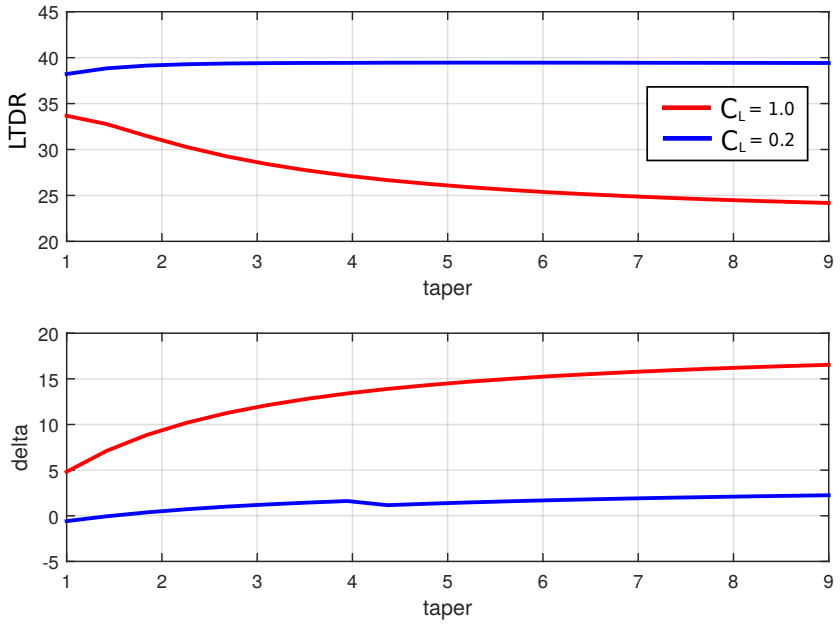

Figure 7.5: Optimal values for lift-to-drag ratio and flap deflection angle as a function of taper.

The first thing to notice looking at Figure 7.5, is that the taper has a smaller influence on the LTDR with respect to sweep angle. About the flight condition with $C_L = 1$ the LTDR tends to slightly decrease. This is understandable considering that increasing the taper with a fixed static margin, the tip chord tends to decrease and so proportionally also the flap chord decrease. In fact the falp is placed at wing tip, the decreasing of flap dimension imply a bigger deflection angle to ensure the same trimming torque. The bigger deflection increase the pressure drag.

Looking at the top graph of Figure 7.6, is clearly visible as increasing the twist angle from negative values to positive ones the LTDR decrease. This behaviour is a direct result of the lift distribution in spanwise direction, in fact the induced drag is linked to tip vortices which are generated by the pressure difference between upper and lower surface of the wing. This pressure difference is also the one that generate the lift, so less lift near the tip mean weaker vortices and so less induced drag. Indeed with negative values of twist angle the lift near the tip is decreased and so the LTDR is increased.

The flap deflection trend is a direct effect of the fact that, having a negative twist angle the trailing edge goes up like during flap deflection. Vice versa when the twist angle is positive the trailing edge goes down, so with negative

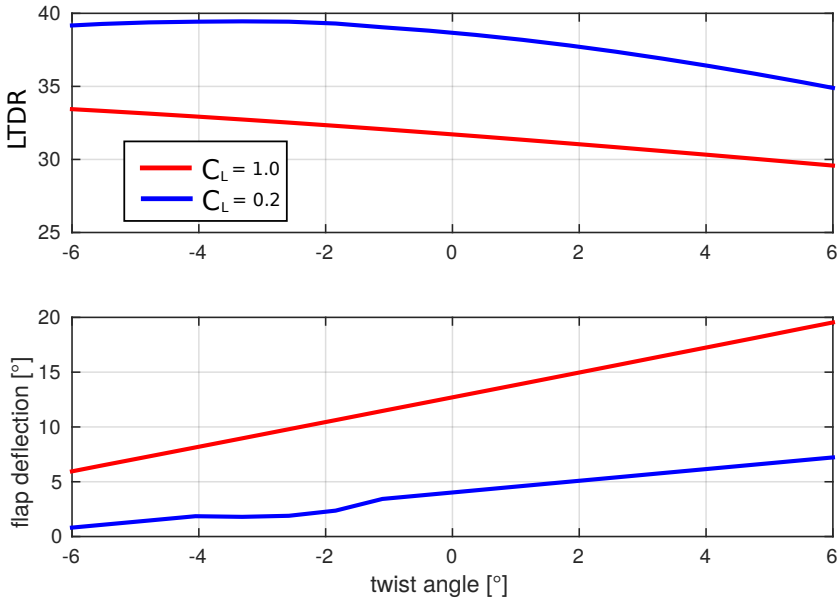

Figure 7.6: Optimal values for lift-to-drag ratio and flap deflection angle as a function of twist angle.

twist angles the flap deflection decrease because some of rotation angle is already performed by the entire airfoil.

7.2 Optimization of Single Part Wing

7.2.1 Problem Description

The goal of this optimization case is to perform constrained drag minimization of a trapezoidal wing, considering horizontal trimmed flight conditions and using the OT implemented in this thesis work.

7.2.2 Baseline Geometry

Single part trapezoidal wing with flaps and with symmetric airfoils refer to Figure 7.7

Wing Parameters :

- Symmetric airfoils NACA 0012;
- Two flaps for half-wing;

- Flaps position and length (Referring to figure 2.10 for the symbols);
  - $s = (10, 55)$ [% of b];
  - $l = (35, 35)$ [% of b].
- Flaps chord 20 [% of wing local chord].

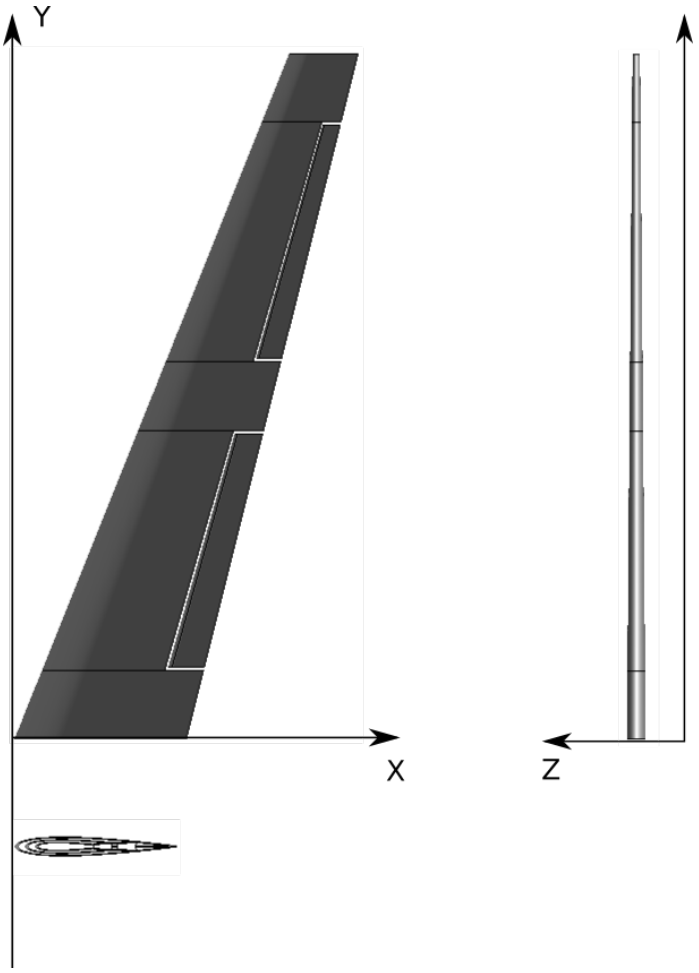

Figure 7.7: Baseline geometry.

The control sections used in the optimization are the root and tip sections.

7.2.3 Mesh Convergence Results

The number of panels and the mesh size are referred to an half-wing.

Looking at the table is easy to notice how mesh M4 could be a good compromise between results accuracy and computational effort restraint. This

Mesh	Mesh size	N_{chord}	$N_{wingspan}$	C_D	C_L	C_M	α
M1	400	20	20	0.028	0.500	-0.565	6.25
M2	1280	40	32	0.027	0.500	-0.577	5.86
M3	2700	60	45	0.021	0.500	-0.579	5.79
M4	4560	80	57	0.013	0.500	-0.581	5.77
M5	7000	100	70	0.011	0.500	-0.581	5.73

Table 7.3: Mesh convergence study results.

because the differences in mesh sizes between M3, M4 and M4, M5 is very similar but the differences in C_D values are instead relevant.

	$\Delta Size$ [% of M4]	ΔC_D [% of M4]
M3,M4	41	61
M4,M5	53	15

Table 7.4: Meshes comparison.

A slow asymptotic stabilization starts from M4 ensuring small variations in C_D values. For this reason M4 has been chosen.

Below are reported the numbers of panels in chord and span direction used in this optimization.

$N_{chord} = 80$

$N_{wingspan} = 57$

7.2.4 Optimization Problem Formulation

The aerodynamic shape optimization seeks to minimize the drag coefficient by varying the shape design variables, the optimization is subjected to several constraints, the most important are :

- Lift coefficient $C_L = 0.2, 1.0$;
- Stati margin $m = \overline{m}$
- Trim $M_{CG} = 0$.

The shape design variables are twist angle of root and tip section, taper ratio, sweep angle and the trimming variables : angle of attack and flaps deflections.

Initial population has been chosen in order to have all the individuals identical to each other and as far as possible to the credible optimized solution. This is due to the necessity to highlight the good performance of the OT.

The complete optimization problem is described in Table 7.5. The quantities reported in the table are referred to only half-wing.

	Function/variable	Description	Quantity
minimize	$C_D + PF_i$	Drag coefficient + Penalty functions	
with respect to	γ_1	Twist angle	1
	λ	Sweep angles	1
	Λ	Taper ratio	1
	δ_i^j	Flaps deflections	2
	α_i	Angle of attack	2
		Total design variables	7
subject to these constraints	$C_L = 0.2 - 1$	Lift coefficient	2
	$\gamma_0 = 0^\circ$	Root section's twist angle	1
	$S = const$	Surface	1
	$b = const$	Structural wingspan	1
	$m = 0.05 \cdot c_{mac}$	Static margin	1
	$M_{CG} = 0$	Static equilibrium	1
		Total constraints	7
and with these boundaries	$-7 \leq \gamma_1 \leq 0$	Twist angles	/
	$0 \leq \lambda \leq 40$	Sweep angle	/
	$1 \leq \Lambda \leq 9$	Taper ratio	/
	$-15 \leq \delta_i^j \leq 15$	Flaps deflections	/
	$0 \leq \alpha \leq 18$	Angle of attack	/
with this starting point	$\gamma_{1,2}^i, \lambda_{1,2}^i, \Lambda_{1,2}^i, (\delta_1^{1,2})^i,$ $, (\delta_2^{1,2})^i, \alpha_1^i, \alpha_2^i$	Individuals	70

Table 7.5: Schematic descripion of the optimization problem.

7.2.5 Results and Comments

After 75 generation and 5250 objective function evaluations, the optimization was terminated. The reason for the termination was the magnitude of the variation of fitness function between two sequential generations, which had decreased below 10^{-6} .

The top graph in Figure 7.8 shows how the optimizer has been worked reducing the objective function.

All the terms present in the legend of the top graph are explained below :

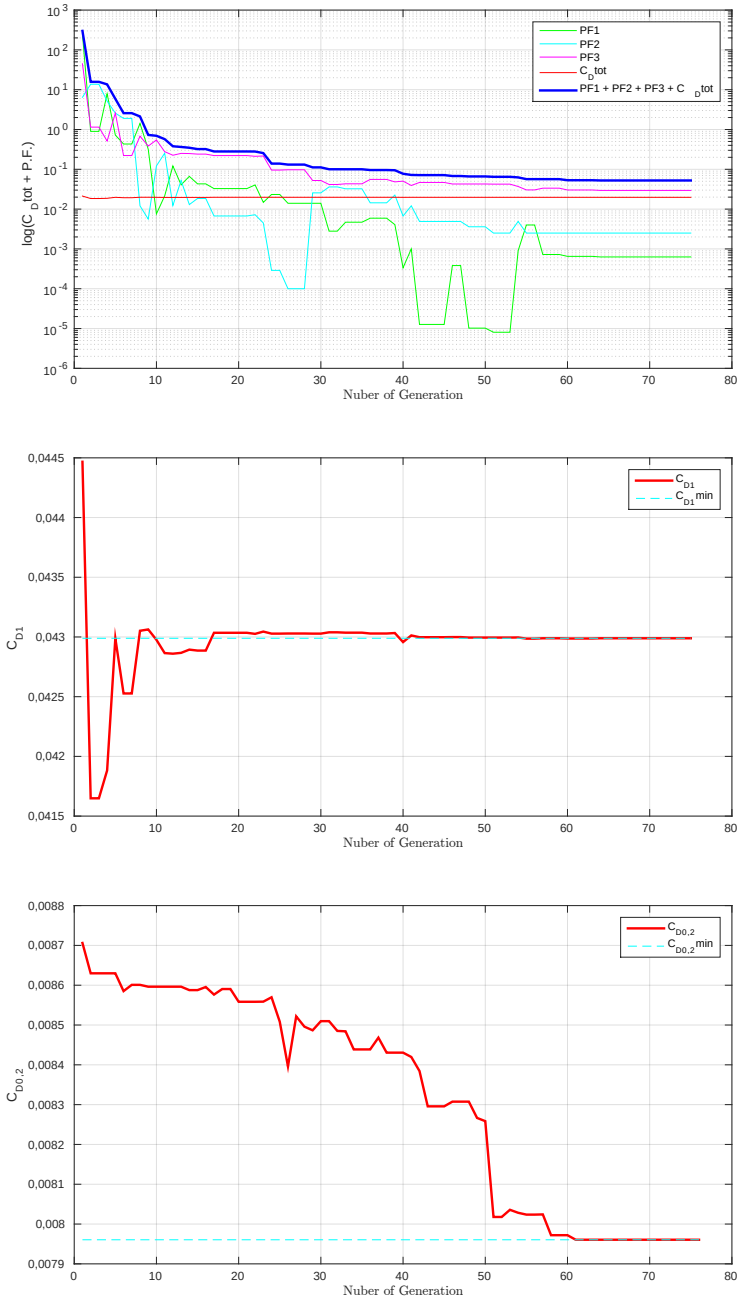

Figure 7.8: Objective function and drag coefficients trend during optimization

- PF1 is the sum of penalty functions calculated at the two flight conditions ($C_L = 0.2, 1$) concerning the static margin constraint;

- PF2 is the sum of penalty functions calculated at the two flight conditions ($C_L = 0.2, 1$) concerning the imposed Lift coefficient;

- PF3 is the sum of penalty functions calculated at the two flight conditions ($C_L = 0.2, 1$) concerning the static equilibrium constraint;
- C_{Dtot} is the sum of the C_D at $C_L = 0.2$ an of C_D at $C_L = 1$.

The second and third graph show the trends of C_D values during the optimization. The second one is referred to C_D evaluated at $C_L = 1$ and the third one is referred to C_D evaluated at $C_L = 0,2$. The trends are very different, in particular looking at the case with $C_L = 1$ it looks like in contrast with a minimization procedure. In fact it decreases suddenly in the initial iterations but then it increases stabilizing at a certain value. This behavior is caused by the constraints, they "guide" the solution in certain directions which not always match with C_D minimization requirement.

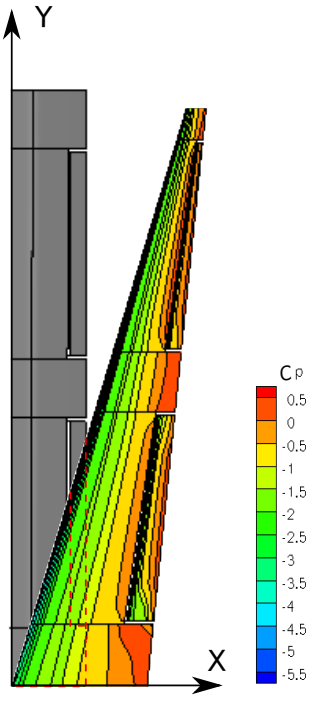

	Initial population		*optimized*
sweep	0.1°	⇒	17.0°
taper	1.0	⇒	7.0
twist	-0.1°	⇒	-3.0°

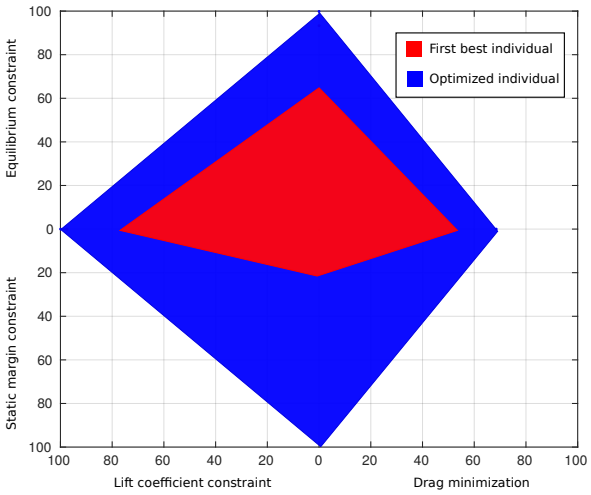

Figure 7.9: Comparison between the initial and the resultingwing geometry after the optimization.

From Figure 7.9 it is clear that the optimizer has tried to get the highest possible aspect ratio. This has been accomplished by reducing a lot the tip chord and consequently increasing the root chord dimension that became bigger with respect the initial individual. This procedure is needed in order to maintain the total surface S constant. This has increased the taper ratio from 1 to 7, with the most likely result of reducing the induced drag.

Also the increase of twist angle absolute value has the aim of reducing the induced drag, in fact increasing the washout the lift near the tips is reduced, reducing at the same time the intensity of tip vortices which cause the induced drag.

The radar graph is very important to understand how better is the optimized individual with respect to the individuals of first generation. It gives a "global" idea of optimization goodness considering that it takes care about all the optimization aspects : function of merit and constraints violation.

In fact on the axes are reported the percentages of how much a constraint is respected and how much the C_D is close to ideal C_{Dmin} obtained using the theoretical formula $C_{Dmin} = C_{D0} + \frac{C_L^2}{\pi ARe}$ where e is the *span efficiency factor* that for elliptical distribution is equal to 1. C_{D0} is taken from airfoil polar knowing the C_L at which the optimization has been performed.

In this particular case the RG show very well that the constraints are perfectly followed and the C_D is quite good. It is also very easy to notice the global improvement obtained by OT, comparing the areas of the the two graphs.

7.3 Optimization of a Wing Composed by Two Trapezoidal Parts

7.3.1 Problem Description

The goal of this optimization case is to perform constrained drag minimization of a wing composed by two trapezoidal parts, considering horizontal trimmed flight and using the OT implemented in this thesis work.

7.3.2 Baseline Geometry

Wing composed by two trapezoidal parts with flaps and with symmetric airfoils refer to Figure 7.10.

Wing Parameters :

- Symmetric airfoils NACA 0012;
- The two patches have the same length;
- Two flaps for half-wing;

- Flaps position and length (Referring to figure 2.10 for the symbols);
  - $s = (10, 55)$ [% of b where b is total structural wing-span];
  - $l = (35, 35)$ [% of b].
- Flaps chord 20 [% of wing local chord];

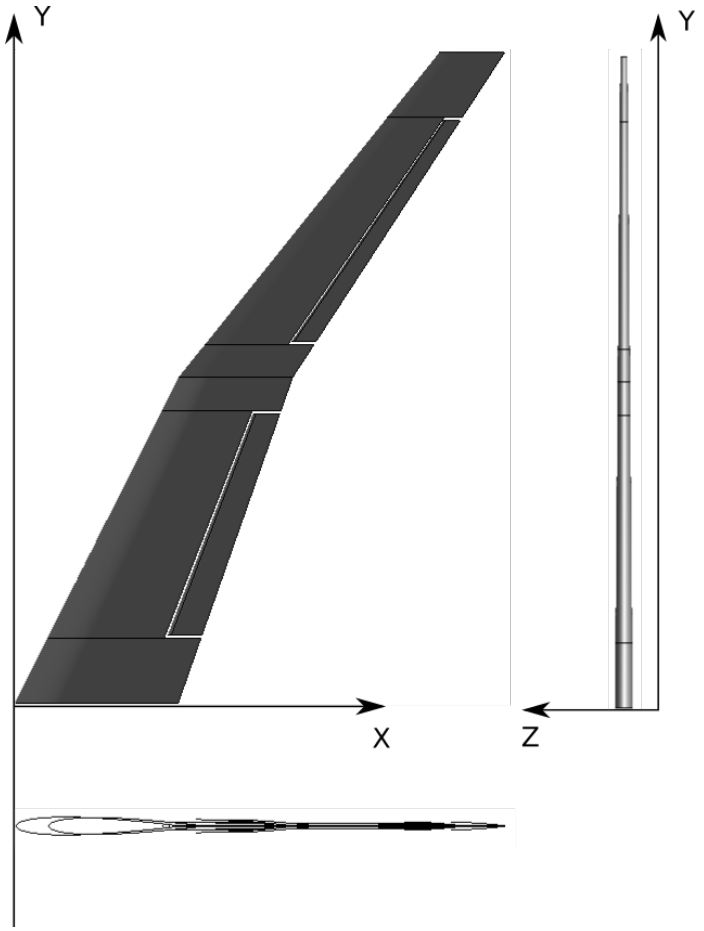

Figure 7.10: Baseline geometry.

The control sections used in the optimization are the root and tip sections of each part.

7.3.3 Mesh Convergence Results

The number of panels and the mesh size are referred to an half-wing.

Following the same considerations made for the previous optimizations, M3 has been chosen.

Mesh	Mesh size	N_{chord}	$N_{wingspan}$	C_D	C_L	C_M	α
M1	550	25	22	0.030	0.500	-0.566	6.20
M2	1548	43	36	0.022	0.500	-0.578	5.82
M3	3250	65	50	0.012	0.500	-0.582	5.78
M4	4950	90	55	0.011	0.500	-0.591	5.74
M5	8580	110	78	0.010	0.500	-0.591	5.70

Table 7.6: Mesh convergence study results.

Below are reported the numbers of panels in chord and span direction used in this optimization.

$N_{chord} = 65$

$N_{wingspan} = 50$

7.3.4 Optimization Problem Formulation

The aerodynamic shape optimization seeks to minimize the drag coefficient by varying the shape design variables, the optimization is subjected to several constraints, the most important are :

- Lift coefficient $C_L = 0.2, 1.0$;
- Stati margin $m = \overline{m}$
- Trim $M_{CG} = 0$.

.

The shape design variables are twist angle, taper ratio, sweep angle for each part and the trimming variables : angle of attack and flaps deflections.

Initial population has been chosen in order to have all the individuals identical to each other and as far as possible to the credible optimize solution.

The complete optimization problem is described in Table 7.7. The quantities reported in the table are referred to only half-wing.

7.3.5 Results and Comments

After 143 generation and 14300 objective function evaluations, the optimization was terminated. The reason for the termination was the magnitude of the variation of fitness function between two sequential generations, which had decreased below 10^{-6} .

	Function/variable	Description	Quantity
minimize	$C_D + PF_i$	Drag coefficient + Penalty functions	
with respect to these constraints	$\gamma_{1,2}$	Twist angle	2
	λ_i	Sweep angles	2
	Λ_i	Taper ratio	2
	δ_i^j	Flaps deflections	2
	α_i	Angle of attack	2
		Total design variables	10
subject to these constraints	$C_L = 0.2 - 1$	Lift coefficient	2
	$\gamma_0 = 0^\circ$	Root section's twist angle	1
	$S = const$	Surface	1
	$b = const$	Structural wingspan	1
	$m = 0.05 \cdot c_{mac}$	Static margin	1
	$M_{CG} = 0$	Static equilibrium	1
		Total constraints	2
and to these boundaries	$-7 \leq \gamma_{1,2} \leq 0$	Twist angles	/
	$0 \leq \lambda_{1,2} \leq 40^\circ$	Sweep angle	/
	$1 \leq \Lambda_{1,2} \leq 9$	Taper ratio	/
	$-15 \leq \delta_i^j \leq 15$	Flaps deflections	/
	$0 \leq \alpha \leq 18$	Angle of attack	/
with this starting point	$\gamma_{1,2}^i, \lambda_{1,2}^i, \Lambda_{1,2}^i, (\delta_1^{1,2})^i,$ $, (\delta_2^{1,2})^i, \alpha_1^i, \alpha_2^i$	Individuals	100

Table 7.7: Schematic descripion of the optimization problem.

- PF1, PF2, PF3, C_{Dtot} have the same meaning as in Section 7.2.

The top graph in Figure 7.11 shows very well the monotonic reduction of the objective function that indicate a good behaviour of the OT. The graphs concerning the C_D trends show an increase, but as already said for the results of the previous optimization, this is not always bad but means that in order to accomplish the constraints the OT has to modify the wing geometry in such a way that the drag is increased.

From Figure 7.12 what is very intersting to note is that, "tip part" is very tapered and has a bigger sweep angle with respect the "root part". The fact that the sweep angle increase towards the wing tip is very important because means that the OT is able to counteract the sweep effect. In the following Section a deeper discussion will be made.

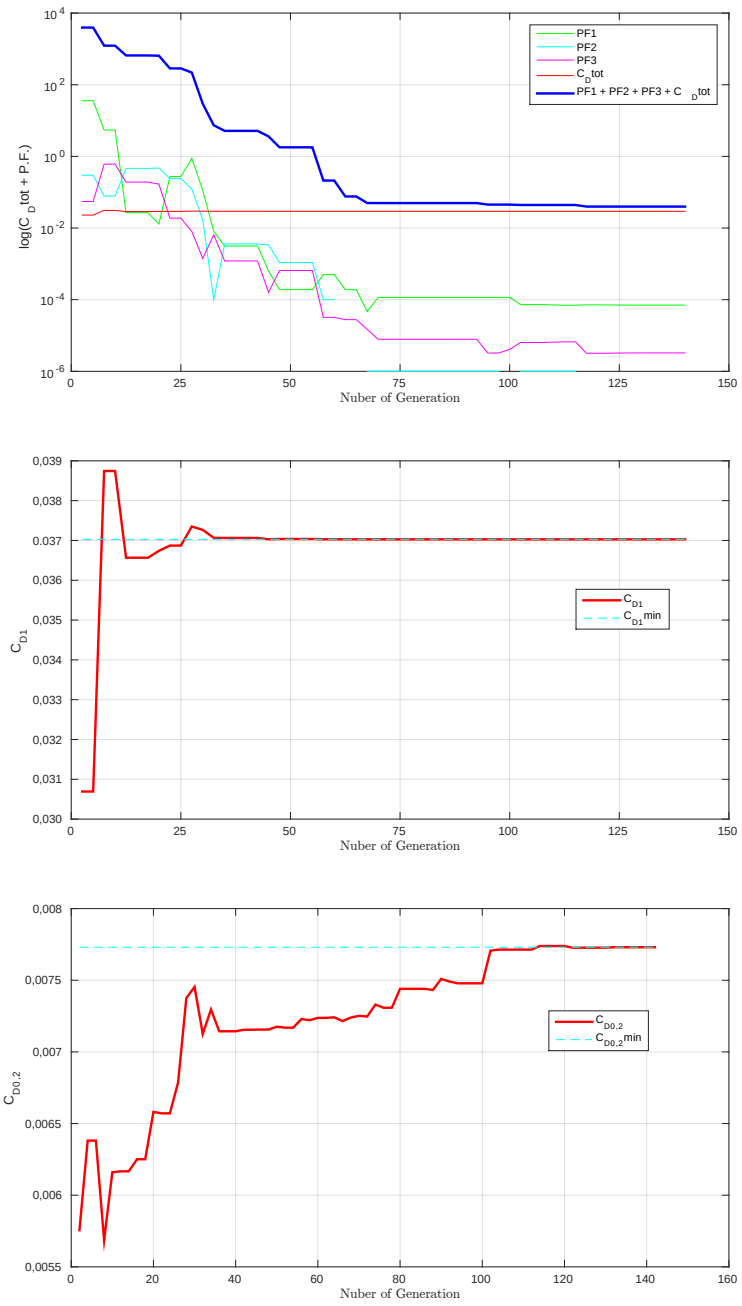

Figure 7.11: Objective function and drag coefficient trend during optimization.

The twist angle became more negative towards the tip, this indicate an increasing washout that helps the taper to reduce the induced drag.

The RG shows very well how the constraints are perfectly satisfied and the C_D is better with respect single part wing.

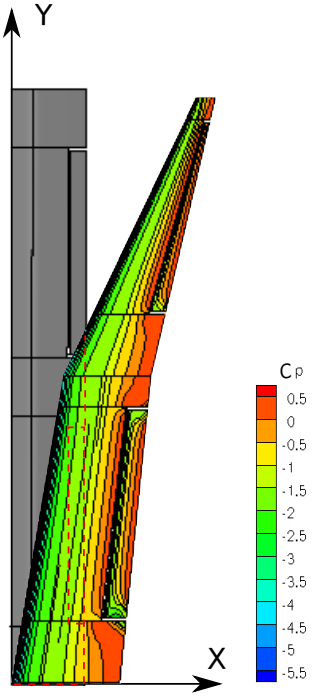

	Initial population			*optimized*	
	root part	tip part		root part	tip part
sweep	0.1°	0.1°	⇒	9.0°	26.0°
taper	1.0	1.0	⇒	1.2	4.7
twist	-0.1°	-0.1°	⇒	-2.5°	-3.5°

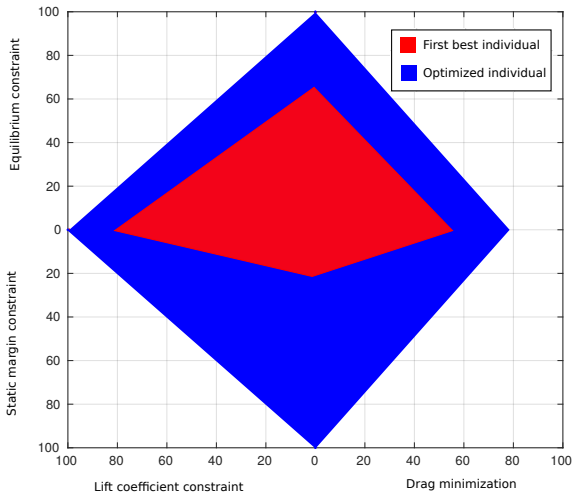

Figure 7.12: Comparison between the initial and the resultingwing geometry after the optimization.

7.4 Analysis of Optimization Results

In this Section the results of Application Studies are compared in order to discuss some intresting aspects that help to understand the OT characteristics.

7.4.1 Sweep Effect

When looking at the wing-span lift coefficient distrubution for wings with different sweep angles Λ, one observes a local decrease of the lift for positive Λ values at the bend, i.e. in the "wing centre". Some times this is called "*lift valley*". The larger the sweep angle is the more the local lift is reduced near the wing centre and the more extended to both sides is the reagion of lift loss.

In the Figure 7.13, two lift distributions are compared. The right one is about the optimized single part wing, the left one is about the optimized double parts wing. The two lift distributions have been obtained considering a trimmed flight condition with an imposing C_L of 1.

What is interesting to notice is the different shape of lift distributions near the

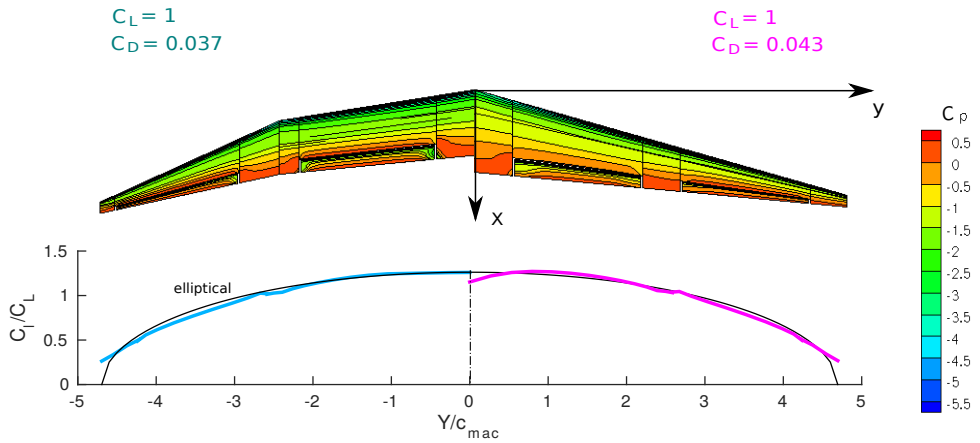

Figure 7.13: Comparison of lift distributions

wing center. The LD on the left has a very smooth shape near the wing root and approach the root horizontally like the elliptical shape. Instead the LD on the right shows a "lift valley" near the root, this peculiarity compromises the optimality of LD distancing it from elliptical shape and increasing the drag coefficient.

This difference in the two LDs is caused by the different sweep angle at the wing center. In fact for the single part wing this angle is 17° instead for the other is 10°; obviously this value is about the "root part", because for what concern the "tip part", the sweep angle is 26°. This configuration allows the two parts wing geometry to have the same static margin as the single one, avoiding at the same time the loss of lift near the wing center. Ensuring a more efficient LD and so a smaller C_D. Obviously this improvement can be larger increasing the number of parts and varying their length in order to have more degree of freedom and perfectly aproximate the elliptical LD.

The LDs in the Figure are not perfectly smooth, these irregularity are due to the presence of ailerons which alter the wing shape and ensure the trim. Despite these irregularity the LDs are not so different from elliptical one, confirming the OT goodness.

7.4.2 Performances Comparison

An interesting analysis could be made comparing the two optimized wing, using the LTDR and Power Index $\rightarrow \frac{C_L^{3/2}}{C_D}$ trends function of C_L. With the number 1 is denoted the wing composed by a single trapezoidal part, the wing denoted with the 2 is the double parts trapezoidal wing.

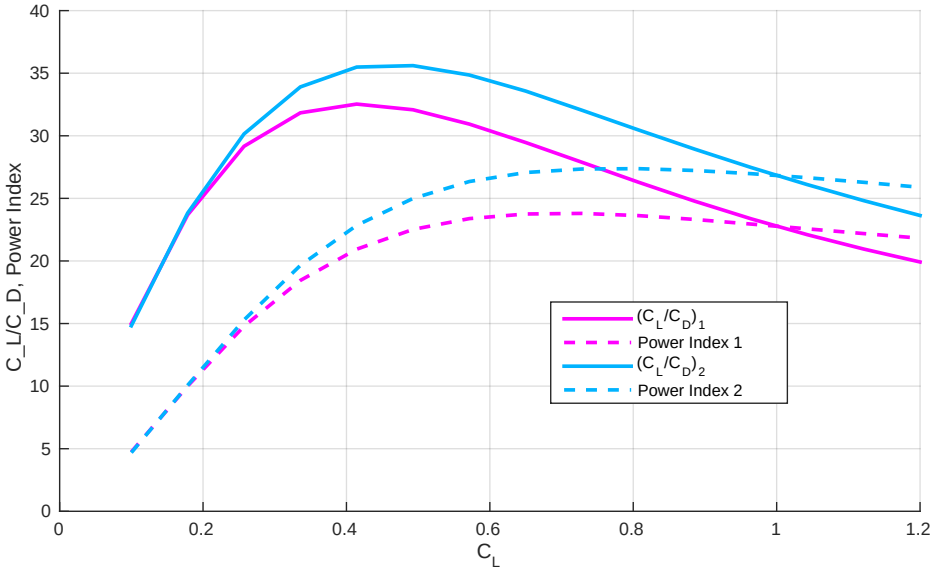

Figure 7.14: Performance comparison

Looking at the Figure 7.14 it is clear that the more "efficient" C_l distribution of wing 2 have an impact on performance. In particular, considering that we are speaking about sailplane, the very important parameter is the Power Index which is an index of merit about sink velocity. Indeed where $\frac{C_L^{3/2}}{C_D}$ is high the sink velocity is low.

Another important thing to notice is about how LTDR is distributed along the different flight conditions. In particular considering which the two wings have been optimized with the aim of find the best compromise between drag coefficients at two flight conditions : $C_L = 0.2$ and $C_L = 1$, their LTDR should be high and uniform with all the lift coefficients between 0.2 and 1. In fact looking at the graph above, $\frac{C_L}{C_D}$ has almost the same value at the two flight conditions, and it is a pretty high value considering the maximum achived along all the range of flight conditions. This fact highlights that the code is able to optimize a flying wing for a certain range of flight conditions.

Considering what said above about sink velocity, it is easy to understand the Figure 7.15 in which the sink velocity is plotted againts horizontal one. Obviously wing 2 that has the better LTDR with respect to wing 1, will have also a lower sink velocity.

The differences between the two velocities are more significant where the V_h is low and so the C_L is high, and they have the tendency to overlap at lower C_L. In the same way this aspect is clearly visible in the graph of Power Index

$$tan(\theta) = \frac{C_D}{C_L}$$

$$V_v = \frac{C_D}{C_L^{3/2}} \sqrt{\frac{2W}{\rho S}}$$

$$V_h = \frac{tan(\theta)}{V_v}$$

$$\frac{W}{S} = 255 \ [N/m^2]$$

$$\rho = 1.225 \ [kg/m^3]$$

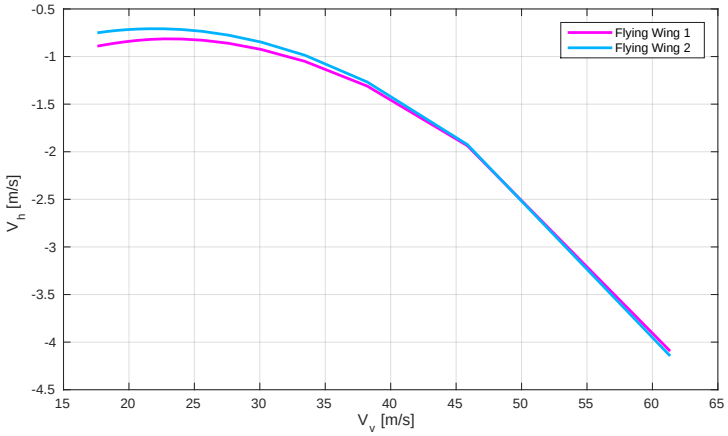

Figure 7.15: Hodograph for glide performance at a given altitude

and LTDR. This is probably caused another time by the differences in C_l distributions. In fact at high C_L the induced drag is a relevant part of the total one and it is mainly caused by C_l distribution, explaining in this way the differences between the performance of the two wings. Instead its importance decreases at high C_L uniforming the performance.

Chapter 8

Conclusions

8.1 Concluding Remarks

In this Thesis the implementation of an Optimization Tool (OT) to design and optimized tailles aircrafts has been presented. Probably the most time consuming and challenging part of the work has been the mesh generator (MEG) implementation. In fact it must be able to generate numerous different geometries with the minimum possible number of variables, it has to be robust, avoiding as much as possible spurius fluctuations and has to be compatible with the aerodynamic solver. All these requirements have driven MEG implementation, first of all the choice to use the Partial Differentila Equation (PDE) method which is pretty complicated to implement but it is very powerful. This method is not very applied in technical papers and documentation, so the bibliography is poor and this has complicated the implementation and tuning.

The MEG tuning has been performed in order to fit it to work with the aerodynamic solver COMPA. Once the two codes have been ready to work together, the optimizer has been chosen. The genetic algorithm (GA) has been selected because the solution space was unknown and probably it would have contained a certain number of local minima which could have impeded a gradient based optimizer. This is a good choice from what regards the possibility to find the global minimum, but is very expensive from a computational point of view. This reduces the computational effort but increases the complexity in the fine tuning of the algorithm. In fact it has been used the GA implemented in Matlab, but many parameters have been changed, in order to adapt the optimizer to this particular problem. This tuning, together with the MEG implementation, has represented the critical aspect of the entire work.

In order to validate and test the OT, some simulations have been performed and presented. First of all there was the necessity to understand if all the components would have worked well together and if the optimization problem was well-set in term of predefined constraints and objective function. This has been accomplished validating the OT, comparing theoretical results with numerical ones. The validation has produced good results, highlighting the goodness of the OT.

This has been the starting point for an "optimization campaign", in order to collect as many results as possible and become familiar with the solution space, with the aim of understand the sensibility of the problem with respect to number and nature of variables and parameters.

Other two optimizations have been performed, for which an etire Thesis section has been dedicated for each one of them, in order to analize deeply the results. The results speak about performance improvements and observance of constraints. In particular an interesting comparison between the results of the two optimizations has been performed. It highlights some peculiarities regarding the relation between sweep angle and spanwise C_l disribution. In this case the optimizer has been able to modify the sweep angle of the "two part wing", in order to avoid a lift decrease near the wing root and so improving the performances.

Obviously there are some criticalities, firstly the computational effort needed, secondly a quite complicated tuning of GA parameters. In fact the aerodynamic solver COMPA has to invert matrices that are proportional to mesh dimesion, so considering an optimization performed with a mesh at convergence and so with many panels, the matrix inversion has became computational expensive. For this particular problem there are not so many solutions because if results must be as accurate as possible, the mesh has to be at convergence, and in general it is composed by a big number of panels. The GA tuning is not an easy task to solve, and together with computational effort they present the biggest issues which have slowed down the OT implementation.

8.2 Future Developments

A summary of the Future Developments will be presented, taking into consideration some points on which future work an analysis might expand.

Optimization Tool:

- Include the use of a Viscid Aerodynamic Solver to comprehend viscid effect in the computation of Aerodynamic coefficients.
- Improve the set up of GA, modifying the crossover function, Elite count, etc
- Improve the way to build up the GA first generation, in order to reduce the Computational Time.
- Try to replace GA with a gradient-based optimizer.
- Include a Stability Augmentation System to extend the optimization domain
- Include a better estimation of structural weight and inertia features.

References

[1] K. Nickel, M. Wohlfahrt. "Tilless Aircraft in Theory & Practice". American Institute of Aeronautics and Astronautics, 1994.

[2] D. Gyorgyfalvy. " Performance analysis of the Horten IV flying wing". In 8th Congress of the Organisation Scientique at Thecnique Internationale du Vol a Voile, Cologne, Germany, 1966.

[3] I. Kroo. "Design and development of the swift : a foot-launched sailplane". AIAA paper 00-4336, 2000.

[4] Hicks, R. M. and Henne, P. A., "Wing Design by Numerical Optimization," *Journal of Aircraft*, Vol. 15, 1978, pp. 407–412.

[5] D. F. Hidalgo Lopez, C. N. Londono, J. I. Garcia Sepulveda. "Low cost aerodynamic optimization for light aviation finite wing using pattern search and apame 3D panel code". *3rd CTA-DLR Workshop on Data Analysis & Flight Control,* September 14-16, 2009, S. J. Campos, SP, Brazil.

[6] S.J. Morris. "Integrated aerodynamic and control system design for tail-less aircraft". In Member AIAA the American Institute of Aeronautics, editor, AIAA *Guidance, Navigation ans Control Conference*, 1992.

[7] M. I.G. Bloor, M. J. Wilson. "Generating parametrizations of wing geometries using partial differential equations". Computer Methods in Applied Mechanics and Engineering, 148 (1997) 125-138.

[8] G. Droandi and G. Gibertini. "Assessment of a Propeller Model Embedded on a Panel Method Code for Aircraft Aerodynamics". *The Journal of Aerospace Science, Technology and Systems*, Vol. 91, No 3/4, September-December 2012, pp. 98-108.

[9] J.L. Hess "Calculation Of Potential Flow About Arbitrary Three Dimensional Lifting Bodies", Douglass-McDonnell, Report MDC J5679–01, October, 1972.

[10] J. L. Hess and A. M. O. Smith "Calculation Of Potential Flow About Arbitrary Bodies", Progress in Aeronautical Sciences, Vol. 8, pp. 1–138, 1967.

[11] B. Maskew and F. A. Woodward "Symmetrical Singularity Model For Lifting Potential Flow Analysis", Journal of Aircraft, Vol. 13, No. 9, pp. 733–734, 1976.

[12] L. Morino, G. Bernardini and M. Gennaretti "A Boundary Element Method For The Aerodynamic Analysis Of Aircraft In Arbitrary Motions", Computational Mechanics, Vol. 32, pp. 301–311, 2003.

[13] M. I. G. Bloor and M. J. Wilson. "Using partial differential equations to generate free-form surfaces". *Computer-Aided Design*, Vol. 22, No 4, May 1990, pp. 202-212.

[14] M. Liu, Y Hu. "The multi-disciplinary robust optimization for tail-less aircraft". In the American Institute of Aeronautics and Astronautics, editors, 15th AIAA/ISSMO *Multidisciplinary Analysis and Optimization Conference*, 2014.

[15] M. Padulo, J. Maginot, M. Guenov, C. Holden. "Airfoil design under un-certainty with robust geometric parameterization". In 50th AIAA/AS- ME/ASCE/AHS/ASC *Structures, Structural Dynamics, and Materials Conference*, Palm Springs, California, 2009.

[16] M. I.G. Bloor, M. J. Wilson. "Efficient parametrization of generic aircraft geometry". *Journal of Aircraft*, Vol. 32, No. 6, pp. 1269-1275, November-December 1995.

[17] J. Mariens. "Wing shape multidisciplinary design optimization". Master of science thesis, Delft University of Technology, August 2/2012.

[18] S. J. Morris, I. Kroo. "Aircraft design optimization with multidisciplinary performance criteria", AIAA-89-1265, April 1989.

[19] N. E. Sevant, M. I. G. Bloor, M. J. Wilson. "Aerodynamic design of a flying wing using response surface methodology". *Journal of Aircraft*, Vol. 37, No. 4, July-August 2000.

[20] B. N. Pamadi. “Performance, Stability, Dynamics, and Control of Airplanes”. American Institute of Aeronautics and Astronautics, 2004.

[21] X. Huang, K. K. Pippalapalli, B. Chudoba. “Aerodynamic snalysis of a Class II high-performance hang glider”. *In 44th AIAA Aerospace Sciences Meeting and Exhibit*, Reno, Nevada, 9 - 12 Januar. 2006.

[22] Jangho Park Jaeyoung Choi Christopher Ocheltree Seongim Choi Duck- joo Lee Yeongmin Jo. “Adaptive variable-fidelity aerodynamic analysis and design for tailless aircraft under model-form uncertainty”. *In 16th AIAA/ISSMO Multidisciplinary Analysis and Optimization Conference*, Dallas, TX, 22-26 June 2015.